Title

Location-Specific Facilitation in Marmoset Auditory Cortex

Authors

Chenggang Chen[+], Sheng Xu[+], Yunyan Wang, and Xiaoqin Wang*

Affiliations

Laboratory of Auditory Neurophysiology, Department of Biomedical Engineering, Johns Hopkins University School of Medicine, Baltimore, Maryland 21205, USA.

[+] Co-first author

Contact information

*Correspondence to: xiaoqin.wang@jhu.edu

Abstract

Responses of auditory cortex neurons are modulated by spectral or temporal context, but much less is known about modulation by spatial context. Here, we investigated single neuron responses to sequences of sounds either repeatedly delivered from a single spatial location or randomly delivered from multiple spatial locations in the auditory cortex of awake marmosets. Instead of inducing adaptation as expected from well-documented stimulus-specific adaptation studies, repetitive stimulation from a target speaker evoked long-lasting, location-specific facilitation (LSF) in many neurons, irrespective of the visibility of the target speaker. The extent of LSF decreased with decreasing presentation probability of the target speaker. Intracellular recordings showed that repetitive sound stimulation evoked sustained membrane potential depolarization which gave rise to firing rate facilitation. Computational models suggest two distinct neural mechanisms underlying LSF. Our findings revealed a novel form of contextual modulation in the auditory cortex that may play a role in auditory stream segregation.

Main

It has been well established that responses of neurons in auditory cortex are influenced by stimulus context. Contextual effects could be suppressive or faciliatory. For example, the presence of a preceding masker sound could suppress a neuron's responses to a succeeding probe sound (Calford and Semple, 1995; Wehr and Zador, 2005; Scholes et al., 2011; Phillips et al., 2017). Preceding stimuli can also facilitate a neuron's responses to succeeding stimuli in auditory cortex under particular conditions (Brosch et al., 1999; Brosch and Schreiner, 2000; Bartlett and Wang, 2005). Contextual modulations can occur in spectral domain (Suga et al., 1979; Sutter and Schreiner, 1991; Nelken et al., 1994; Feng and Wang, 2017), temporal or spectrotemporal domain (O'Neill and Suga, 1979; Kilgard and Merzenich, 2002; Brosch and Scheich, 2008; Sadagopan and Wang, 2009; Asari and Zador, 2009).

In addition to spectral and temporal context, spatial context can also modulate sound processing in auditory cortex. For example, responses of neurons in macaque auditory cortex elicited by a stimulus with 0° interaural phase disparity (IPD) may be altered by preceding stimuli with 90° or -90° IPD (Malone et al. 2002). Responses of neurons to a probe sound from one spatial location could be suppressed by masker sounds from other locations (Fitzpatrick et al., 1999; Reale and Brugge, 2000; Mickey and Middlebrooks, 2005). In a study of awake marmoset primary auditory cortex (A1) and adjacent caudal field, it was found that a masker placed far away from a neuron's spatial receptive field (SRF) can suppress the response elicited by a probe sound in its SRF, suggesting widespread contextual modulations in the spatial domain (Zhou and Wang, 2012, 2014). However, comparing to spectral and temporal contextual effects, much less is known on spatial contextual effects in auditory cortex.

An important property of auditory cortex neurons is that they exhibit stimulus-specific adaptation (SSA) to the stimuli that are presented with a high probability (Nelken, 2014). SSA has attracted much interest in the past two decades (Malmierca and Auksztulewicz,

2021) because it was thought to be a potential neuronal correlate of mismatch negativity (MMN) (Ulanovsky et al., 2003; Fishman and Steinschneider, 2012), which has been extensively studied in humans (Näätänen et al., 2007) and is believed to reflect deviance detection (Polterovich et al., 2018; Pérez-González et al., 2021) and predictive coding (Parras et al., 2017; Carbajal and Malmierca, 2018), etc. SSA has been studied mostly in spectral (Nelken et al., 2013; Natan et al., 2015; Harpaz et al., 2021) and temporal (Awwad et al., 2020) domains. It is not clear to what extent SSA exists in the spatial domain.

In this study, we explored how spatial contextual modulations evolve by stimulating neurons in the awake marmoset auditory cortex with sequences of sounds either randomly from various spatial locations (equal-probability mode) or repeatedly from a single location (continuous mode). To our surprise, instead of inducing adaptation as expected from well-documented SSA literature, repetitive stimulation in the high probability mode from spatial locations away from the center of a neuron's SRF evoked lasting facilitation observed by extracellular recordings from single neurons in the auditory cortex. Nearly half of the sampled neuronal population exhibited this spatial facilitation, irrespective of the stimuli type and visibility of the test speaker. The extent of the facilitation decreased with decreasing presentation probability of the test speaker. Intracellular recordings showed that repetitive sound stimulation evoked sustained membrane potential depolarization that was followed by firing rate facilitation. We used computational models to explore neural mechanisms underlying neural facilitation. Taken together, our findings revealed location-specific facilitation (LSF) to repetitively presented sound stimuli in auditory cortex that has not been observed. This form of spatial contextual modulation may play a role in such functions as detecting the regularity, segregating the sound stream, and solving the cocktail party problem.

Results

Repetitive sound stimulation evoked neural facilitation

We evaluated how extracellularly recorded individual neurons in the auditory cortex responded to broadband sounds played from different speaker locations. Fifteen equally spaced speakers were placed on a semi-spherical surface centered around the animal's head and above the horizontal plane (Fig. 1a, b). In each test session, we first probed a neuron's spatial selectivity by delivering a frozen wideband noise stimulus from each speaker location in a randomly shuffled order. We will refer to this stimulation mode as the *equal-probability presentation mode* for which all locations have the same occurrence probability of 1/15. Spatial receptive field (SRF) was constructed for each neuron using the averaged firing rate of the responses to wideband noises in the equal-probability presentation mode. Fig. 1c, d show the responses of an example neuron obtained in the equal-probability presentation mode. This neuron had an SRF centered around speaker #7 (Fig. 1c) and responded to this location with sustained firing throughout the stimulus duration, and to other locations with onset or transient firing (Fig. 1d). Fig. 2a shows firing rate versus speak number for the equal-probability presentation mode. Speaker #7

evoked the highest firing rate (38.5 spikes/sec) in this neuron, followed by speaker #8 (10.5 spikes/sec). Speakers #14, #13, #9 and #11 evoked near zero firing rate, and a negative firing rate was observed for speakers #2, #4, and #5. Because the firing rate for each speaker location is calculated by subtracting the spontaneous firing rate from the total firing rate, a negative firing rate indicates inhibition.

After the characterization of a neuron's SRF, we further tested each neuron with the *continuous presentation mode* in which stimuli were delivered from a speaker location repeatedly, with each trial separated by an inter-stimulus interval of fixed or variable length (range: 500 to 5200 ms, see below). Fig. 2b, c show the responses of the same neuron depicted in Fig. 1c, d and Fig. 2a to 300 presentations of a 200 ms frozen wideband noise stimulus delivered from speaker #14 in the continuous presentation mode. Speaker #14 evoked 0.8 spikes/sec firing rate in the equal presentation mode (Fig. 2a, blue dot) which was considered as the baseline firing rate of this speaker location. In contrast to the expectation from previous auditory cortex literature on adaptation, the response of this neuron to the repeated presentations of a wideband noise stimulus from the same speaker #14 showed epochs consisting of consecutive trials with substantially higher firing rates than the baseline firing rate (median: 16 spikes/sec, Fig. 2c, red dots). Elevated firing rates could be observed in trials long after the first trial (e.g., between 150th and 250th trials). Also note that during the trials with elevated firing rates (Fig. 2b, red dots), the firing patterns were sustained throughout the stimulus duration. To further examine the facilitated response in the continuous presentation mode, we measured the "facilitation phase" to characterize trials with firing rates exceeding the facilitation threshold which was defined as one standard deviation above the baseline firing rate (Fig. 2a, c, orange bar). This neuron exhibited several facilitation phases lasting up to 42 trials (Fig. 2c, red dots). Fig. 2d-f show responses of another example neuron. In the equal-probability presentation mode, this neuron had weak responses to marmoset vocalization stimuli at speaker #8 (Fig. 2d, blue dot, 0.05 spikes/sec). When tested in the continuous presentation mode with speaker #8 (Fig. 2e, f), this neuron had weak responses initially, but the responses gradually built up and eventually led to a facilitation phase (median: 4.8 spikes/sec) lasting 20 trials (Fig. 2f, red dots).

Neural facilitation occurred in a variety of stimulus conditions

We tested a total of 104 auditory cortex neurons in four hemispheres of three marmosets using wideband stimuli including frozen wideband noises, amplitude-modulated wideband noises, and marmoset vocalizations. 725 sessions were tested by both equal-probability and continuous presentation modes. Population statistics of the facilitation phase are shown in Extended Data Fig. 1a which shows that a facilitation phase could persist as long as 45 trials. For further analyses, we focused on the sessions that exhibited facilitation phases lasting at least 5 consecutive trials (129 sessions from 51 neurons). In the majority of sessions, 200 trials were tested (Extended Data Fig. 1b). In most sessions, it took fewer than 100 trials to achieve the first facilitation phase lasting at least 5 consecutive trials (median: 44 trials) (Extended Data Fig. 1c).

We calculated the proportion of facilitation trials in the continuous presentation mode

for the 129 sessions from 51 neurons that exhibited facilitation phases lasting at least 5 consecutive trials which ranged between 15%-87.5% (median: 32.8%) (Fig. 3a, orange line). As a control, we also calculated the proportion of facilitation trials in the equal-probability presentation mode for the same group of 51 neurons (Fig. 3a, blue line) which was significantly smaller than that of the continuous presentation mode (14.3% vs. 32.8%, $p < 0.0001$, rank-sum test). The group of 51 neurons scattered across all recorded cortical areas and did not show any clustering patterns (Extended Data Fig. 2a-d). Most of the neurons (43/51) were recorded at superficial cortical depths (< 1 mm, Extended Data Fig. 2e, f). We attempted to distinguish putative excitatory and inhibitory neurons by their spike waveform (broad or narrow; Extended Data Fig. 3a) (Mitchell et al., 2007). Spike waveform of 32 neurons had been recorded and 29 neurons had a signal-to-noise ratio higher than 20 dB (Extended Data Fig. 3b). 23 neurons were classified as putative excitatory neurons (yielded 58 sessions) and 6 neurons as putative inhibitory neurons (yielded 12 sessions) (Extended Data Fig. 3c). The proportions of facilitation trials were similar between putative inhibitory and excitatory neurons (Extended Data Fig. 3d; 34% vs. 32%, $p = 0.2271$, rank-sum test). This analysis suggests that the facilitation can be induced in both putative excitatory and inhibitory neurons.

We conducted control tests to see if the observed facilitation depended on visual inputs. We found that the facilitation was not limited to speakers located within a marmoset's visual field (< 90 degrees) (Chaplin et al., 2012) and could be induced from speaker locations both in front and behind an animal (Extended Data Fig. 4a-c). Across all 129 test sessions, the proportions of facilitation trials were similar between front (64 sessions) and back (65 sessions) speaker locations (Fig. 3b; 38% vs. 35%, $p = 0.4653$, rank-sum test). The facilitation could still be observed when an animal was tested in the darkness (7 sessions) (Extended Data Fig. 4d-f). Interestingly, the proportion of facilitation trials was significantly higher in the darkness than in the light-on condition (122 sessions) (Extended Data Fig. 4g; 57% vs. 32%, $p < 0.0001$, rank-sum test). These results suggest that visual inputs are not required to induce the facilitation. We also tested the effects of different stimulus types. Neural facilitation was also observed using unfrozen wideband noises (Extended Data Fig. 4h). Comparing to frozen wideband noises (83 sessions), slightly larger proportion of facilitation trials was observed using complex stimuli including amplitude-modulated frozen wideband noises (37 sessions) or marmoset vocalizations (9 sessions) as stimuli (Fig. 3c; 30% vs. 41%, $p = 0.0054$, rank-sum test).

Neural facilitation was observed at both short inter-stimulus intervals (ISI) (700 ms, Fig. 2b) and long ISI (1900 ms, Fig. 2e). In addition to ISI with a fixed length, we also tested random ISIs in a subset of sessions. An example is shown in Extended Data Fig. 5a. This neuron not only showed facilitation at three constant ISIs but also at random ISIs. Across all 129 test sessions, three groups of ISIs were tested: short (500 ms and 700 ms, 78 sessions), long (>1000 ms, 36 sessions) and random (700 ms to 2200 ms, 15 sessions). The proportion of facilitation trials was similar between the three ISI groups (Extended Data Fig. 5b; 35%, 41%, and 34%, $p = 0.1244$, one-way ANOVA).

Neural facilitation did not alter a neuron's SRF

Previous studies in both auditory and visual cortices found that after presenting a stimulus repeatedly, neurons typically exhibited a decrease of response to the stimulus but an increase of response to other stimuli that are sufficiently different from the repeated stimulus (Condon and Weinberger, 1991; Dragoi et al., 2000), which suggests changes in a neuron's receptive field. To investigate whether neural facilitation altered a neuron's SRF, we compared the SRF measured before and after testing a neuron in the continuous presentation mode. An example neuron is shown in Extended Data Fig. 6a (same neuron in Fig. 1c). After presenting 300 trials of wideband noise at the same location continuously (spike raster shown in Fig. 2b), the SRF (Extended Data Fig. 6a, bottom) appeared similar to the SRF measured before (Extended Data Fig. 6a, top). More examples of pre and post SRFs are shown in Extended Data Fig. 6b. To quantitatively characterize SRF changes, we calculated three metrics in 61 neurons in which pre and post SRFs were measured: tuning selectivity, direction selectivity, and correlation coefficient. The average tuning selectivity (Extended Data Fig. 6c, left, 0.153 vs. 0.146) and direction selectivity (Extended Data Fig. 6c, right, 0.477 vs. 0.473) remained similar after tested by the continuous presentation mode. To further quantify the tuning similarity, we computed the pairwise correlation coefficient between each pair of responses to fifteen speaker locations (Extended Data Fig. 6d, left). 75% (197/262) of pair of sessions had a correlation coefficient greater than 0.7 (Extended Data Fig. 6d, right). We also examined if firing rate changed after a neuron was tested by the continuous presentation mode for the highest (1st) and lowest (15th) ranked target speakers (Extended Data Fig. 6e). Both speaker ranks showed similar firing rates before and after being tested by the continuous presentation mode (ranked 1st: 13.8 vs. 13.0 spikes/sec; ranked 15th: 2.9 vs. 2.6 spikes/sec), consistent with the observations on SRF stability (Extended Data Fig. 6a-d). These analyses show that the repetitive presentation of stimuli from the same speaker location does not significantly alter the SRF of the neuron being tested.

In the 129 sessions that exhibited facilitation phases lasting for at least 5 consecutive trials when tested by the continuous presentation mode, the average firing rate during the facilitation phases was nearly three times greater than that evoked by the same speaker location under the equal-probability presentation mode (Extended Data Fig. 6f, orange box: 17.5 vs. 6.6 spikes/sec, $p < 0.0001$, one-way ANOVA). The spontaneous firing rates during equal-probability presentation mode, non-facilitation and facilitation phases of the continuous presentation mode were similar (Extended Data Fig. 6f, blue box: 5.1, 5.2, and 6.2 spikes/sec, $p = 0.3924$, one-way ANOVA). Thus, the facilitation phases during the continuous presentation mode were not accompanied by significant changes in spontaneous activities.

Neural facilitation depends on sound locations

Neural facilitation was observed at all tested speaker locations. To investigate the effect of speaker location on the facilitation, each speaker was assigned a rank number based on its baseline firing rate obtained under the equal-probability presentation mode. Speaker ranked 1st had the highest firing rate among all tested speakers and was at or near the center of a neuron's SRF. The lowest ranked speaker usually fell far outside of

the SRF and evoked a response not significantly different from the spontaneous activity. The speaker rank of an example neuron is shown in Fig. 3d. We found that speakers with lower ranks usually elicited more facilitation phases than speakers with higher ranks when tested under the continuous presentation mode as shown by the example neuron in Fig. 3e, orange dots. Note that in this neuron no facilitation was induced by the frontal speaker (speaker #1, rank 5th) and only one facilitation trial (out of 200 trials) was induced by the speaker at the contralateral 90° location (speaker #6, rank 4th). These two locations were commonly used in previous SSA studies (see Discussion). When the test speaker was ranked 15th, 18 of 77 (23.4%) tested sessions had facilitation phases lasting for at least 5 consecutive trials (Extended Data Fig. 7a) and the average proportion of facilitation trials was 21.6% (Fig. 3f, orange dots). In comparison, when the test speaker was ranked 1st, these statistics dropped to 10.5% (4/38 tested sessions, Extended Data Fig. 7a) and 7.3% (Fig. 3f, orange dots), respectively.

In addition to the facilitation, suppressed responses were also observed in the continuous presentation mode. We measured the “adaptation phase” to characterize trials with firing rates lower than the adaptation threshold which was defined as one standard deviation below the baseline firing rate (Fig. 3d, blue bar). At higher ranked speakers, more adaptation phases were observed than at lower ranked speakers as shown by an example neuron in Fig. 3e, blue dots. Note that 70% of trials (140/200) exhibited adaptation at the frontal speaker (speaker #1, rank 5th) and 52.5% of trials (105/200) showed adaptation at the contralateral 90° location (speaker #6, rank 4th). The average proportion of adaptation trails across all tested sessions was 26.1% when the test speaker was ranked 1st, whereas that number dropped to 8.9% when the test speaker was ranked 15th (Fig. 3f, blue dots). This trend was the opposite of facilitation (Fig. 3f, orange dots).

Neural facilitation primarily depends on sound location but not firing rate

We showed above that neural facilitation depends on speaker rank, which was determined by firing rate in the equal-probability presentation mode at a neuron’s preferred sound level. Sound level was a crucial parameter to influence the firing rate of auditory cortex neurons (Sadagopan and Wang, 2008; Wang, 2018). This gives us the opportunity to determine whether the neural facilitation primarily depends on sound location or any type of stimuli that could influence the firing rate, including speaker location and sound level. Therefore, we measured a neuron’s responses to wideband noise delivered from fifteen speaker locations at four sound levels under the equal-probability presentation mode in a subset of neurons. An example of this analysis is shown in Fig. 4a. We assigned this neuron a speaker rank and sound level rank. In contrast to previous figures where the speaker rank was determined by firing rate at one sound level (mostly the best sound level), the speaker rank in this analysis was determined by the averaged firing rate (Fig. 4a, black dots) at four sound levels (Fig. 4a, four different color dots). The sound level rank at each speaker location was also determined by the firing rate in which the 1st ranked sound level had the highest firing rate among the four tested sound levels. If the neural facilitation was location-dependent,

then the facilitation shall increase from higher ranked speakers to lower ranked speakers, but not from higher ranked sound levels to lower ranked sound levels. If the neural facilitation was firing rate-dependent, then the facilitation shall increase from higher ranked speakers to lower ranked speakers as well as from higher ranked sound levels to lower ranked sound levels.

We performed the speaker rank and sound level rank analysis in 390 sessions obtained from 63 neurons. At each sound level rank, the proportion of facilitation trials tended to be larger at the lower ranked speakers (Fig. 4b, fifteen same color dots in x-axis). When averaged across sound levels, the proportion of facilitation trials was only 3.4% at the speaker ranked 1st (21 sessions tested) whereas the proportion jumped to 19.1% when the test speaker was ranked 15th (41 sessions tested) (Fig. 4b, slope of northeast arrow; Extended Data Fig. 7b, orange dots). In contrast, at each speaker rank, the proportion of facilitation trials did not vary much when the sound level rank changed (Fig. 4b, four different color dots in y-axis). When averaged across speakers, the proportion of facilitation trials was 12.4% at the sound level ranked 1st (119 sessions tested) whereas the proportion rose slightly to 13.4% when the sound level was ranked 4th (61 sessions tested) (Fig. 4b, length of upwards arrow; Extended Data Fig. 7c, orange dots).

Compared to neural facilitation, the proportion of adaptation trials tended to be larger at both higher ranked speakers (Fig. 4c, fifteen same color dots in x-axis) and higher ranked sound levels (Fig. 4c, four different color dots in the y-axis). When averaged across sound levels, the proportion of adaptation trials was 18.0% at the speaker ranked 1st and the proportion dropped to 8.9% when the test speaker was ranked 15th (Fig. 4c, slope of southeast arrow; Extended Data Fig. 7b, blue dots). When averaged across speakers, the proportion of adaptation trials was 18.5% at the sound level ranked 1st and the proportion dropped to 12.3% when the sound level was ranked 4th (Fig. 4c, length of downwards arrow; Extended Data Fig. 7c, blue dots).

These results suggest that neural facilitation is primarily dependent on sound location, but not firing rate. In contrast, neural adaptation is primarily dependent on firing rate which is expected from previous adaptation literature.

Dependence of neural facilitation on location continuity

As we have shown above, neural facilitation can be induced in the continuous presentation mode in which the probability of stimuli delivered from a target speaker is 100% (none from other speakers). In the equal-probability presentation mode, the presentation probability for each speaker is equal to 1/ 15 (number of speakers). Therefore, the continuous presentation mode provides the location continuity for sound delivery, whereas the equal-probability presentation mode does not. We further investigated in a subset of units whether the sound location continuity was necessary to induce neural facilitation by changing the presentation probability of the target speaker from 100% to 75%, 50%, 25% and 6.7% (Fig. 5a, target speaker: orange square; other speakers: blue color shapes). An example neuron is shown in Fig. 5b. The decrease of the target speaker's presentation probability to 75%, 50%, and 25% resulted in increasingly weaker responses of the target speaker (100%: 20, 75%: 20, 50%: 10, and

25%: 6 spikes/sec). Across all 57 test sessions in 12 neurons, the decrease of the presentation probability of the target speaker from 100% to 75%, 50%, 25% and 6.7% resulted in weaker response of the target speaker (6.81, 3.43, 1.93, 1.89 and 0.88 spikes/sec, Fig. 5c) and the reduction of the proportion of facilitation trials (44%, 23%, 16%, 21% and 14%, Fig. 5d). The proportion of facilitation trials lasting for at least 5 consecutive trials showed a similar trend of decrease (Fig. 5e, 25%, 12%, 5%, and 0%).

Previous stimulus-specific adaptation (SSA) related studies found that neurons in the auditory cortex of anesthetized rats were sensitive to statistical regularities: standard and deviant tones in random sequences both evoked larger responses than the same tones in periodic sequences (Yaron et al., 2012; Parras et al. 2017). To investigate whether neural facilitation is also sensitive to the statical regularity of the target speaker, we played two different types of sequences with 50% probability of the target speaker. In one sequence, stimuli from the target speaker and other speakers were randomly arranged, similar to the 75%, 25%, and 6.7% probability mode (Fig. 5a, 50). In the other sequence, stimuli from the target speaker were interleaved with stimuli from other speakers, so that the stimuli from the target speaker were periodical (Fig. 5a, 50/p). In contrast to SSA, we found that the periodic target speaker sequence evoked significantly stronger responses than the random target speaker sequence (Fig. 5c, 3.91 vs. 1.93 spikes/sec, $p = 0.0443$, rank-sum test). The proportions of facilitation trials were similar between random and periodic target speaker sequence with 50% probability. (Fig. 5d-e).

Repetitive sound stimulation induced sustained membrane potential depolarization

We next asked what are cellular mechanisms underlying the neural facilitation evoked by repetitive stimuli. In a subset of experiments, we performed intracellular recordings in awake marmoset (Gao et al. 2016; Gao and Wang, 2019) to examine both membrane potential and spiking activity during both equal-probability presentation and continuous presentation modes. Fig. 6a shows membrane potential traces of an example neuron. Fig. 6b shows the speaker rank based on firing rate obtained under the equal-probability presentation mode in this neuron. Our previous analyses of the spiking activity measured the “facilitation phase” to characterize trials with firing rates exceeding the facilitation threshold which was defined as one standard deviation above the baseline firing rate (Fig. 2a, 2d, 3d, and 6b, orange bar). Here, we measured the “depolarization phase” to characterize trials with membrane potential exceeding the depolarization threshold which was defined as one standard deviation above the baseline membrane potential (Fig. 6c, blue bar). The membrane potential steadily increased after 40 trials during the continuous presentation (Fig. 6d, blue line) which was accompanied by an increase in spiking activity (Fig. 6d, orange line).

We conducted 30 sessions under the continuous presentation mode in 14 intracellularly recorded neurons at different speaker locations. The target speakers were divided into a low ranked group (10th to 15th) and a high ranked group (1st to 6th). For the low ranked group, we observed a larger proportion of depolarization trials than hyperpolarization trials (Fig. 6e, gold dots, 43% vs. 19%, $p = 0.1810$, rank-sum test). In contrast, the opposite trend was observed for the high ranked group (Fig. 6e, violet dots,

7% vs. 50%, p = 0.0044, rank-sum test). Thus, both the firing rate facilitation and membrane potential depolarization were influenced by the speaker rank. We further calculated the membrane potential variation of each trial. Trials were classified into depolarization, hyperpolarization, or transition groups based on whether they passed the depolarization threshold, hyperpolarization threshold, or neither. Depolarization trials had the lowest variation and hyperpolarization trials had the highest variation (Fig. 6f, 1.07 vs. 2.97, p < 0.0001, one-way ANOVA).

For each session, we compared the difference between the number of trials needed to achieve the first membrane potential depolarization phase and the spiking facilitation phase that lasted for at least 5 consecutive trials. We found that the depolarization of membrane potential always preceded the facilitation of spiking activity (Fig. 6g, median: 9 trials). Fig. 6h shows changes in membrane potential magnitude after depolarization (seven sessions). The resting membrane potential was -69 mV. After 30 trials, membrane potential achieved a stable level of -62 mV which was 7 mV depolarized. We will use these three parameters in our computational models below.

Computational models suggest two distinct neural mechanisms underlying location-specific facilitation

Our in vivo extracellular and intracellular recording data showed that both spiking and subthreshold activity of a neuron could be modulated (facilitation or adaptation of spiking activity and sustained depolarization or hyperpolarization of membrane potential) by repetitive stimuli in a location-specific way. We used two computational models to investigate potential neural mechanisms underlying these observations. In our models, synaptic inputs were panoramic (i.e., with inputs from every spatial location) based on observations from previous whole-cell recording studies in rats. Chadderton et al. (2009) found excitatory postsynaptic potential (EPSP) could be evoked from all spatial locations in all tested neurons. Kyweriga et al. (2014) found excitatory and inhibitory currents could be evoked by all interaural level difference (ILD) cues. Panoramic inputs make it possible for a cortical neuron to generate neural facilitation or sustained depolarization by amplifying weak responses at unpreferred sound locations.

A conceptual model for location-specific facilitation and adaptation in spiking activity is shown in Extended Data Fig. 8a. In this model, a neuron receives panoramic excitatory and inhibitory inputs but with varying strengths according to the speaker ranking as revealed by the equal probability presentation mode (upper plot). When stimuli are repetitively presented at the 15th-ranked speaker (right plot), stronger inhibitory inputs to the model neuron would result in larger depression than the depression of weaker excitatory inputs (Extended Data Fig. 8c). The overall stronger excitation than inhibition would evoke neural facilitation at this speaker location (Extended Data Fig. 8e). When stimuli are repetitively presented at the 1st-ranked speaker (left plot), stronger excitatory inputs to the model neuron would result in a larger depression than the depression of weaker inhibitory inputs. Then the overall stronger inhibition than excitation would evoke neural adaptation at this speaker location. We call this neuron model “EI-LIF model” in which excitatory and inhibitory inputs are differentially depressed (Fig. 7a).

A second conceptual model is shown in Extended Data Fig. 8b for membrane

potential. This model is based on the idea that the brain state is modulated when stimuli switch from equal-probability presentation mode to continuous presentation mode (see Discussion). Since neural activity of the network is homeostatically regulated (Pacheco et al. 2019), sustained depolarization of weaker responses (red line) at the 15th ranked speaker will be accompanied by sustained hyperpolarization of stronger responses (blue line) at the 1st-ranked speaker. A sustained depolarization makes it easier to reach the threshold thus evoke neural facilitation (Extended Data Fig. 8d, e). In contrast, a sustained hyperpolarization makes it harder to reach the threshold thus evokes neural adaptation. We call this neuron model "MP-LIF model".

Fig. 7b, c, f, g show the neural facilitation simulated with the EI-LIF model (up) and MP-LIF model (down) in the continuous presentation mode. Notice the elevated firing rates were observed in tens of trials after the start of continuous sound stimuli (Fig. 7b, f, red dots) and epochs consisting of consecutive trials with higher firing rates than the facilitation threshold (Fig. 7c, g, red lines). We also simulated neural adaptation in the EI-LIF model (Extended Data Fig. 8f) and MP-LIF model (Extended Data Fig. 8g). The threshold of neural facilitation and adaptation were calculated in the equal-probability presentation mode (gray area). Notice the sparse spikes (Extended Data Fig. 8f, g, blue dots) and epochs consisting of consecutive trials with firing rates lower than the adaptation threshold (Extended Data Fig. 8f, g, blue line).

We further examined whether our models could also simulate the speaker probability-dependent neural facilitation observed in Fig. 5. We hypothesized that the recovery time of excitatory and inhibitory synaptic release and amplitude of sustained membrane potential depolarization were proportional to the probability of the target speaker (Fig. 7a, e). We found that decreasing the target speaker's presentation probability reduced the proportion of facilitation trials in the EI-LIF model (Fig. 7d, gold dots) and MP-LIF model (Fig. 7h, gold dots). Two models' performances were close to the experimental results observed in Fig. 5d (now shown as Fig. 7d, h, green dots). We further compared the proportion of facilitation trials in our models with 129 experimentally tested sessions in the continuous and equal-probability presentation mode shown in Fig. 3a (now shown as Fig. 7d, h, red dots). The results were also similar at 100% and 6.7% probabilities (EI-LIF: 39% vs 36% and 18% vs 14%; MP-LIF: 41% vs 36% and 18% vs 14%). In summary, both EI-LIF and MP-LIF models recapitulated the neural facilitation and adaptation observed in our experiments and suggest potential underlying neural mechanisms. Future experimental studies can provide validations of these suggested mechanisms.

Discussion

In this study, we investigated extracellular and intracellular neural responses to repetitive sound stimulation in the auditory cortex of awake marmoset monkeys. The major finding of this study is the observation of a novel location-specific facilitation (LSF) which is dependent on sound location and stimulus presentation mode. LSF raises questions on the conventional definition of the spatial receptive field as being a static

property of a auditory cortical neuron. LSF is a different phenomenon than the well-studied stimulus-specific adaptation (SSA). Computational models based on the synaptic depression or sustained depolarization mechanisms can both reproduce the LSF. The dependence of facilitation on location continuity and regularity suggests that LSF is a potential single-neuron substrate of auditory streaming.

Implications for the spatial receptive field (SRF) of cortical neurons

The concept of a stable spatial receptive field (SRF) has been a cornerstone of our understanding of spatial tuning in the central auditory system. Auditory cortex neurons in anesthetized animals exhibit predominantly broad SRFs that typically increase in size (or width) as sound level increases (Middlebrooks and Pettigrew 1981; Mrsic-Flogel et al. 2005). In contrast, studies in awake animals have reported restricted SRFs which do not increase or show less increase in size as sound level increases (Mickey and Middlebrooks 2003; Woods et al. 2006; Zhou and Wang, 2012; Remington and Wang, 2019). It has been shown that behavior engagement could further decrease the size of SRFs and therefore sharpen spatial tuning of cortical neurons (Lee and Middlebrooks, 2011; van der Heijden et al., 2018). The finding of the present study further showed that the spatial tuning of auditory cortex neurons in awake marmosets is not static in that a non-preferred spatial location could become responsive under particular conditions. This suggests that cortical neurons can respond to spatial locations away from the center of SRF dynamically. When stimuli from other locations were inserted into the repetitively presented sound sequence from one location, neural facilitation was interrupted and even diminished (Fig. 5). However, neurons still preserve their original SRF after being presented with repetitive sound stimuli (Extended Data Fig. 6). In contrast, after a repetitive pure tone stimulus was presented, a neuron changes its spectral receptive field by reducing responses to the specific tone frequency (Condon and Weinberger, 1991). A non-static SRF could play a role in spatial and binaural tuning plasticity that are observed in monaural deprived animals (Popescu and Polley, 2010; Keating et al., 2015).

Comparison with stimulus-specific adaptation (SSA)

Adaptation to repetitive sound stimulation (i.e., a reduction in response to a high-probability stimulus) by auditory neurons is a commonly observed phenomenon and has been referred to as stimulus-specific adaptation (SSA) (Harpaz et al., 2021; Malmierca et al., 2014; Nelken, 2014). In previous studies that demonstrated SSA, both close field and free field sound stimulation paradigms were used in anesthetized or awake animals. In close field stimulation, the sound was delivered through a sealed speaker into the contralateral ear (Condon and Weinberger, 1991; Yaron et al., 2012; Hershenhoren et al., 2014; Nieto-Diego and Malmierca, 2016) or preferred ear (Ulanovsky et al., 2004). In free field stimulation, the sound was played from the location contralateral to (Chen et al., 2015; Kato et al., 2015; Natan et al., 2017), in front of (Natan et al., 2015) or above (Farley et al., 2010) an animal. Adaptation to repetitive sound stimulation was also observed in the current study, in particular when stimuli were delivered from preferred sound locations (i.e., higher ranked speaker locations at or near the center of SRF) (Fig. 3e, f) or sound levels (i.e., higher ranked sound levels) (Fig. 4c). However, when sound

was delivered from locations away from the center of SRF, our study revealed neural facilitation to repetitive sound stimulation in the auditory cortex of awake marmosets. To the best of our knowledge, no previous studies have systematically tested repetitive sound stimulation across spatial locations.

The most striking difference between the current study and previous SSA studies is the observation of facilitation instead of adaptation to repetitive stimulation in the auditory cortex. Although the predominant response in auditory system to high probability stimuli is adaptation, unadapted and even facilitated responses have been observed in a few previous studies. Thomas et al. (2012) found that repetitive stimulation did not elicit adaptation in specialized (FM-selective) neurons of bat inferior colliculus (IC). They argued that because in echolocating bats behaviorally relevant sounds are echoes from objects, adaptation to those repetitive echolocation signals that occur with a high probability would be maladaptive during active echolocation. Parras et al. (2017) showed that most neurons on the ascending auditory pathway (IC, auditory thalamus, auditory cortex) of anesthetized rats exhibited repetition suppression. However, repetition enhancement was observed in all three areas. Lesicko et al. 2022 and Kommajosyula et al. 2021 also found repetition enhancement in the IC and auditory thalamus of awake rodents, respectively. This is consistent with our findings that periodic target speaker sequences evoked stronger responses than random target speaker sequences (Fig. 5c).

Together, our finding of neural facilitation to the repetitive sound stimulation provides a complementary contextual modulation effect to the SSA and a new perspective on our current understanding of cortical responses to repetitive stimuli.

Neural mechanisms underlying LSF

We investigated the neural mechanisms underlying LSF with two approaches. Experimentally, we directly recorded the membrane potential from neurons that exhibited LSF in awake marmosets (Fig. 6). Computationally, we built a leaky integrate-and-fire (LIF) neuron model and manipulated its excitatory-inhibitory synaptic depression amplitude and recovery time (EI-LIF model) and membrane potential depolarization or hyperpolarization amplitude (MP-LIF model). Both models reproduced LSF and recapitulated the key properties of LSF (Fig. 7).

Two mechanisms may account for the LSF observed in this study. One is repetitive stimulus-evoked synaptic depression. Although excitatory and inhibitory synapses are both depressed by repetitive stimuli (Galarreta and Hestrin, 1998), inhibitory synapses may show a larger amplitude of depression than excitatory synapses (Heiss et al., 2008). The imbalance between excitation and inhibition may produce LSF. Two lines of evidence support this hypothesis. First, the subthreshold activity could be evoked from all tested sound locations (Chadderton et al., 2009) and strong sound-evoked inhibition is commonly observed outside of the SRF (Zhou and Wang, 2014; Remington and Wang 2019). Therefore, the panoramic and strong inhibitory inputs are more susceptible to depression than excitatory inputs. Second, compared to the excitatory inputs, the inhibitory inputs are more sensitive to context change (Kuchibhotla et al., 2016) and show stronger depression during the forward masking (Wehr and Zador, 2005), suggesting the inhibitory inputs are more adjustable than excitatory inputs. Our EI-LIF model could

reproduce the LSF based on the hypothesis that neuron has a stronger depression of their inhibitory inputs than excitatory inputs, thereby supporting a synaptic depression mechanism.

Another mechanism is salient stimulus-evoked membrane potential depolarization. A salient auditory spectrotemporal feature could attract attention automatically (Kayser et al., 2005; Huang and Elhilali, 2020). A wideband noise used in this study was not salient when it was presented randomly from different locations to characterize SRF. However, a wideband noise could become salient when it was repetitively presented from one location while sounds at all other locations disappeared. This auditory spatial pop-out hypothesis is similar to visual saliency where a visual item in sharp contrast with its neighboring items in a simple feature, such as color or orientation, automatically captures attention (Yan et al., 2018). If a location-specific wideband noise is salient, a more salient sound feature at the spectrotemporal domain, e.g., amplitude-modulated wideband noise and vocalization, indeed evoke a larger proportion of facilitation trials than the less salient unmodulated wideband noise (Fig. 3c). In humans, salient auditory stimuli dilate the pupil (Wang et al., 2014). Pupil dilation is closely correlated with membrane potential depolarization and a decrease in membrane potential variation (McGinley et al., 2015). Interestingly, we observed similar changes in membrane potential when neurons exhibit LSF (Fig. 6), suggesting that the ongoing repetitive stimuli are salient to the animals. Importantly, our MP-LIF model reproduced LSF by incorporating parameters obtained from intracellular recordings. Together, our intracellular recording data and MP-LIF model simulation support a salient stimulus-evoked sustained depolarization mechanism underlying the LSF.

It is not clear whether top-down attention plays a role in LSF. It has been shown that task engagement could modulate the SRFs (Lee and Middlebrooks, 2011). In the current study, marmosets passively listened to sound stimuli, though they might have chosen to pay attention to repeated stimulation from a particular location in the continuous stimulation mode. However, we did not observe an increase in spontaneous activity when neural facilitation was observed (Extended Data Fig. 6f), whereas attention tends to increase spontaneous activity (Luck et al., 1997; Reynolds et al., 2000). Furthermore, we found no preference of different cell types in exhibiting the LSF (Extended Data Fig. 3d), whereas top-down attention has stronger modulation over putative inhibitory neurons (Mitchell et al., 2007).

Candidate neural substrate for auditory streaming

In a natural environment like at a cocktail party, sounds are often simultaneously and continuously generated by multiple sound sources (Cherry, 1953). One major challenge for a listener is forming auditory streaming (McDermott, 2009). Streaming requires acoustic cues such as frequency, temporal regularity, and sound location (Shamma and Micheyl, 2010). Over the past decade, a rapidly increasing number of studies have investigated the effect of temporal regularity or repetition for streaming (Bendixen et al., 2010; Andreou et al., 2011). Regular stimulation induces stronger responses than random stimulation when measured with magneto-electro encephalography (M/EEG) and functional MRI (fMRI) in humans (Barascuda et al., 2016; Southwell et al., 2017). The

findings that repetitive sound stimulation evoked LSF and regular stimulation evoked a stronger response than random stimulation provide a candidate single-neuron correlate of this perceptual phenomenon. Computational modeling suggests that the change of synaptic efficacy could result in sustained responses to regular stimulation (Auksztulewicz et al., 2017). Interestingly, changing the excitatory and inhibitory synaptic efficacy in our EI-LIF model also generated the LSF. Those two models further suggest that sustained response to regular stimulation and LSF share a similar neural mechanism. Repetition causes the target to pop out from the background and is robust to inattention (McDermott et al., 2011; Masutomi et al., 2015). Based on the same pop-out hypothesis, our MP-LIF model could reproduce the LSF. Those similarities suggest that our EI-LIF and MP-LIF models provide a theoretical foundation for both LSF observed in marmosets and enhanced response to regular over random stimulation observed in humans. Together, our findings and models provide valuable new insights into the neural mechanisms of auditory streaming.

Methods

Animal preparation and experimental setup. Data were collected from five hemispheres of four monkeys (Monkey 1: left, Monkey 2: left and right, Monkey 3: right, Monkey 4: left). All experimental procedures were approved by the Johns Hopkins University Animal Use and Care Committee. These procedures were identical to those described in previous publications from our laboratory (Lu et al. 2001). A typical recording session lasted 3-4 h, during which an animal sat quietly in a specially adapted primate chair with its head immobilized. Throughout the entire recording session, the animal was closely monitored via a video camera by the researcher. The eye position was not controlled, but when the animal closed its eyes for a prolonged period, the experimenter ensured the animal opened its eyes before the next stimulus set was presented.

Experiments were conducted in double-walled sound-proof chamber (Industrial-Acoustics) with the internal walls and ceiling lined with three-inch acoustic absorption foam (Sonex). Fifteen free-field loudspeakers were placed on a semi-spherical surface centered around the animal's head and above the horizontal plane. Speaker setup was similar to our previous studies (Zhou and Wang, 2012), but with speakers covered the rear sphere. Eight speakers were evenly positioned at 0° elevation, five speakers were evenly spaced at +45° elevation in the frontal hemifield, one speaker was located at +45° elevation in the rear midline and one speaker located directly above the animal.

Extracellular and intracellular recordings. Extracellular recording procedures were identical to those described in our previous publications. A sterile single tungsten microelectrode (A-M Systems) was hold by a micro-manipulator (Narishige) and inserted nearly perpendicularly into the auditory cortex through a small opening on the skull (1.0–1.1mm in diameter) and advanced by a hydraulic micro-drive (David Kopf Instruments). The tip and impedance of electrode was examined before each recording session (2-5MΩ impedance). Spikes were detected by a template-based spike sorter (MSD, Alpha Omega Engineering) and continuously monitored by the experimenter while data

recordings progressed. The raw voltage signal was also recorded. Intracellular recording procedures were identical to those described in our previous publications (Gao et al. 2016; Gao and Wang, 2019). The recordings were made in the auditory cortex through the intact dura using a concentric recording electrode and guide tube assembly. The sharp recording pipette was made of quartz glass. The guide tube was made of borosilicate glass. The sharp recording pipette was pulled by a laser puller (P-2000, Sutter Instrument), and the guide tube was pulled by a conventional puller (P-97, Sutter Instrument). The electrode assembly was advanced perpendicularly relative to the cortical surface with a motorized manipulator (DMA1510, Narishige). The electrical signals were amplified (Axoclamp 2B, Molecular Devices), digitized (RX6, Tucker-Davis Technologies), and saved using custom programs (MATLAB, Mathworks).

Acoustic stimuli. Four different stimulus presentation designs were used. 1) Continuous (100%): the same stimulus was repeatedly delivered from a fixed speaker location over many trials. 2) Unequal-probability and random (75%, 50%, and 25%): stimulus was delivered from multiple speaker locations in a randomly shuffled order, but target speaker has a higher probability than others. 3) Unequal-probability and periodic (50/p%): stimulus delivered from the target speaker was interleaved with stimulus delivered from other speakers, so that the stimulus delivered from the target speaker was periodical. 4) Equal probability (6.7%): stimulus was delivered from multiple speaker locations in a randomly shuffled order and all speakers shared the same occurrence probability. For each neuron, if allowed by the experiment conditions, the equal-probability presentation mode was tested at multiple separate sessions at different time points and other three presentation modes were tested between the equal-probability presentation mode.

Stimuli were generated digitally in MATLAB at a sampling rate of 97.7kHz using custom software, converted to analog signals (RX6, Tucker-Davies Technologies), attenuated (PA5, Tucker-Davies Technologies), power amplified (Crown Audio), and played from specified loudspeaker. The sound tokens used included unfrozen wide-band noise, frozen wide-band noise, amplitude-modulated wide-band noise and species-specific vocalizations. Sessions collected under continuous unfrozen wide-band noise stimuli were used only in Extended Data Fig. 4h. Fixed inter-stimulus intervals (ISI) were used in four presentation modes. A variety of random ISI were used only in continuous presentation mode. The shortest ISI was 500ms, and the longest ISI was 5200ms. Rate-level function was used to find the best sound level of tested neurons. Most neurons were tested using best sound level, except sound level rank experiments where four different sound levels were used. The same sound level was used when comparing different presentation modes.

Characterization of spatial receptive fields. Total firing rates were calculated over a time window beginning 15ms after stimulus onset and 50ms after stimulus offset. Total firing rates subtracted by the spontaneous rate was the firing rate. SRF characterization was identical to our previous studies (Remington and Wang, 2019). The threshold was the half maximal firing rates. Tuning selectivity was defined as the number of areas that have higher firing rates than the threshold divided by the total number of areas. Direction

selectivity was defined as the product of every area, unit vector and firing rate divided by the product of every area and firing rate. If a neuron only responded to contralateral and ipsilateral 90° at horizontal plane and have equal firing rates, then the direction selectivity was zero. In the plotted SRF, the location of white color dot indicated the preferred sound location, the dot diameter was proportional to the direction selectivity, the black thick line was the half-maximum threshold of SRF, area encircled by the threshold was the reciprocal of tuning selectivity.

Identification of cortical areas, layers and cell types. We used the best frequency (BF) of neurons to identify the subregions of auditory cortex. For the neurons significantly responding to at least one tone stimulus played at the front speaker, we specified the frequency of the tone stimulus that evoked the maximum response rate as the neuron's BF. Marmoset auditory cortex is situated largely ventral to the lateral sulcus and exhibits a topographical frequency gradient along the rostral–caudal axis. The boundary between primary auditory cortex (A1) and the caudal area (caudal-medial and caudal-lateral belt) can be identified by an abrupt decrease of BF at the high-frequency (caudal) border of A1. A1 was further divided into the low-frequency (≤8KHz) rostral A1 and high-frequency (>8KHz) caudal A1 along the rostral-caudal axis. First spike depth was the absolute depth where the first spike was detected from this electrode, and was depended on thickness of dura, variations in granulation tissue, proximity to the curvature of the sulcus, and orthogonality of the electrode penetration to the cortical surface. We used the trough to peak duration of spike waveforms to identify putative excitatory and inhibitory neurons (Mitchell et al., 2007). Before analyzing the spike duration, we calculated the signal to noise ratio of spike waveforms (Sabyasachi and Wang, 2012), which was defined as the action potential peak to peak height divided by the standard deviation of the background noise over 1ms preceding all spikes ($20 \times \log10(AP_{peak-peak}/Noise_{SD})$).

The proportion of facilitation, adaptation, depolarization and hyperpolarization trials. The facilitation phase was defined as the trials whose firing rates were at least one standard deviation above the mean firing rate evoked under the equal-probability presentation mode. The sum of facilitation trials divided by the total trial number in each session was defined as the proportion of facilitation trials. The adaptation phase was defined as the trials whose firing rates were at least one standard deviation below the mean firing rate evoked under the equal-probability presentation mode. To analyze the membrane potential change, spikes were removed from voltage signal with a time window of 3ms centered around the spike peak. The proportion of depolarization and hyperpolarization trials were calculated similar to the proportion of facilitation and adaptation trials.

Speaker rank and sound level rank. Speaker tested in each continuous presentation mode was assigned a rank number based on its firing rate obtained under the equal-probability presentation mode. Speaker ranked 1st and 15th had the highest and lowest firing rate among all 15 speakers tested, respectively. When the SRF has a single peak, speaker ranked 1st and 15th usually had the closest and farthest distance to the

preferred direction, respectively. When the SRF has multiple peaks, low ranked speaker may next to the preferred direction occasionally. We used speaker firing rate rank instead of distance rank for two reasons: one, the SRF of some neurons was quite dispersive, thus it was inaccurate to compute the distance between the target speaker and the SRF center; and two, the SRF center was usually determined by several high ranked speakers. The contribution of low ranked speakers was not considered when using the distance rank. For sound level rank, we measured neurons' responses to 200ms wide-band noise played at four sound levels under the equal-probability presentation mode. These four sound levels were a series of fixed values with an interval of 20dB.

Computational models of location-specific facilitation. Computational models that recaptured the location-specific facilitation (LSF) phenomenon were based on two neural mechanisms (Extended Data Fig. 8a-d): excitatory and inhibitory synaptic depression (EI-LIF model, see equations 4 and 5) and membrane potential depolarization and hyperpolarization (MP-LIF model, see equation 6 and 7). EI-LIF model dynamically changed the depression amplitude of synaptic vesicles release and exponential recovery time constant. MP-LIF model dynamically changed the resting potential and spiking threshold. In the LSF, the parameters were modulated by the probability of presentation speaker, e.g., 100% for continuous presentation mode and 6.7% for equal-probability presentation mode.

The membrane potential V_{t+1} of a leaky integrate-and-fire (LIF) neuron at time step Δt was:

$$V_{t+1} = -\frac{\Delta t}{C}\left[g_{e_t}(V_t - E_e) + g_{i_t}(V_t - E_i) + g_{rest}(V_t - E_{rest})\right] + V_t + \sigma_s\omega_n\sqrt{\Delta t} \quad (1)$$

g_{e_t} and g_{i_t} was the excitatory and inhibitory synaptic conductance (see equations 2 and 3). C, E_e, E_i and g_{rest} was the membrane capacitance, excitatory reversal potential, inhibitory reversal potential, and leak conductance. Those values were obtained from the *in vivo* whole-cell recording in the auditory cortex of anesthetized rats (Wehr and Zador, 2003). Gaussian noise $\sigma_s\omega_n$ was added to generate the spontaneous firing (Lee et al., 2020). Action potential was evoked when the V_{t+1} reached the spike threshold V_{spike}. V_{t+1} was reset to E_{rest} after the action potential. E_{rest} was obtained from our intracellular studies (Fig. 6h). It was fixed in the EI-LIF model but was dynamically modulated in MP-LIF model. V_{spike} is the sum of threshold above resting potential V_{th} and E_{rest}. It was fixed in the EI-LIF model but was modulated in MP-LIF model.

Excitatory conductance g_{e_t} and inhibitory conductance g_{i_t} were:

$$g_{e_t} = P_{rel\_e}rN_e\Delta te^{\frac{\Delta t}{\tau}} + \sigma_c\omega_n \quad (2)$$

$$g_{i_t} = P_{rel\_i}N_i\Delta te^{\frac{\Delta t}{\tau}} + \sigma_c\omega_n \quad (3)$$

P_{rel_e} and P_{rel_i} were the excitatory and inhibitory synaptic release probability, respectively (see equations 4 and 5). P_{rel_e} and P_{rel_i} were modulated in EI-LIF model but fixed to one in MP-LIF model. The inhibitory and excitatory inputs have the same strength and occurred simultaneously, so the inhibitory to excitatory ratio r equal to one and the inhibitory to excitatory delay d (not shown in the equation) equal to zero. The

number of excitatory inputs N_e, inhibitory input N_i and time constant τ were fixed and conduction noise $\sigma_c\omega_n$ was added to generate the spontaneous firing (Wehr and Zador, 2003).

For the EI-LIF model, in each trial T, the excitatory and inhibitory synaptic release probability $P_{rel\_e_{t+1}}$ and $P_{rel\_i_{t+1}}$ were:

$$P_{rel\_e_{t+1}} = 1 + \left((1 - A_e)P_{rel\_e_t} - 1\right) e^{\frac{-\Delta t}{P_s \tau_e}} \quad (4)$$

$$P_{rel\_i_{t+1}} = 1 + \left((1 - A_i)P_{rel\_i_t} - 1\right) e^{\frac{-\Delta t}{P_s \tau_i}} \quad (5)$$

A_e and A_i was the excitatory and inhibitory synaptic depression amplitude, respectively. A_i was larger than A_e because we observed facilitation instead of adaptation in the continuous presentation mode. In addition, Heiss et al., 2008 found that inhibition adapts more than excitation when repetitively stimulating the whisker. A_e and A_i were both fixed in the LSF. Relatively small depression amplitude was chosen due to the slow facilitation processes observed in the recording data.

τ_e and τ_i was the excitatory and inhibitory recovery time constant, respectively. τ_e was longer than τ_i because numerous studies found that inhibitory synapses have a quick recovery than excitatory synapses (Galarreta and Hestrin, 1998; Varela et al., 1999). In the different probability presentation mode, facilitation percent and firing rate decreased when the probability of target speaker decreased. Since the time constant was stimulus frequency dependent (Galarreta and Hestrin, 1998), therefore the τ_e and τ_i were scaled by the presentation probability P_s which resulted in higher synaptic release probability, i.e., less adaptation, when the presentation probability was low. Time constant can across multiple time scales from hundreds of milliseconds to tens of seconds (Varela et al., 1997; Ulanovsky et al., 2004). Since 44 trials were required to reach the first long facilitation phase, τ_e and τ_i were chosen so that the probability of release was stable after 40 trials.

Each session is composed of randomly presented trials T_r for computing the facilitation and adaptation threshold and continuously presented trials T_c for computing the facilitation percent, adaptation percent, and firing rate. The median firing rate in the 100% probability presentation mode was 12 spikes per second. Therefore, the number of stimulus count N_{SC} was chosen so that the average firing rate in the EI-LIF model could match the firing rate in the recording data. Notice that N_{SC} was Poisson distributed and not every stimulus input could evoke a spike output in the LIF neuron. We run EI-LIF model for two hundred sessions for every presentation probability.

For the MP-LIF model, in each trial T, the dynamic resting membrane potential E_{rest_MP} and spike threshold V_{spike} were:

$$E_{rest\_MP} = \begin{cases} E_{rest},\ 1 \le T < T_r \\ E_{rest}: P_s M/(T_{th} - 1): E_{rest} + P_s M,\ T_r + 1 \le T < T_r + T_{th} \\ E_{rest} + P_s M,\ T_r + T_{th} + 1 \le T < T_r + T_c \end{cases} \quad (6)$$

$$V_{spike} = \begin{cases} V_{th} + E_{rest},\ 1 \le T < T_r \\ V_{th} + E_{rest}: P_s MS/(T_{th} - 1): E_{rest} + P_s MS,\ T_r + 1 \le T < T_r + T_{th} \\ V_{th} + E_{rest} + P_s MS,\ T_r + T_{th} + 1 \le T < T_r + T_c \end{cases} \quad (7)$$

The depolarization value M and the number of trials to reach the stabilized depolarization value T_{th} were obtained from our intracellular recordings. Since lower presentation probability evoked less neural facilitation, therefore M was scaled by the presentation probability P_s. Spike threshold V_{spike} was further modulated by the spike threshold scale S. Almost no spike was evoked when S equal to one but excessive spikes were evoked when S equal to zero. Therefore, S and stimulus count N_{SC} were chosen so that the average firing rate matched the recording data. We also run MP-LIF model for two hundred sessions at every presentation probability. Extended Data Table. 1 listed the names of parameters and corresponding values used in EI-LIF and MP-LIF model neurons

Data availability

Source data for generating Fig. 1 to Fig. 7 has been uploaded to the manuscript tracking system for review purposes. All the data will be freely accessible upon publication.

Code availability

Codes (MATLAB R2022a) for generating Fig. 1 to Fig. 7 and computational models have been uploaded to the manuscript tracking system for review purposes. All the codes will be freely accessible upon publication. Codes (MATLAB R2012a) for controlling the TDT sound presentation and data acquisition system are freely available upon request from the corresponding author.

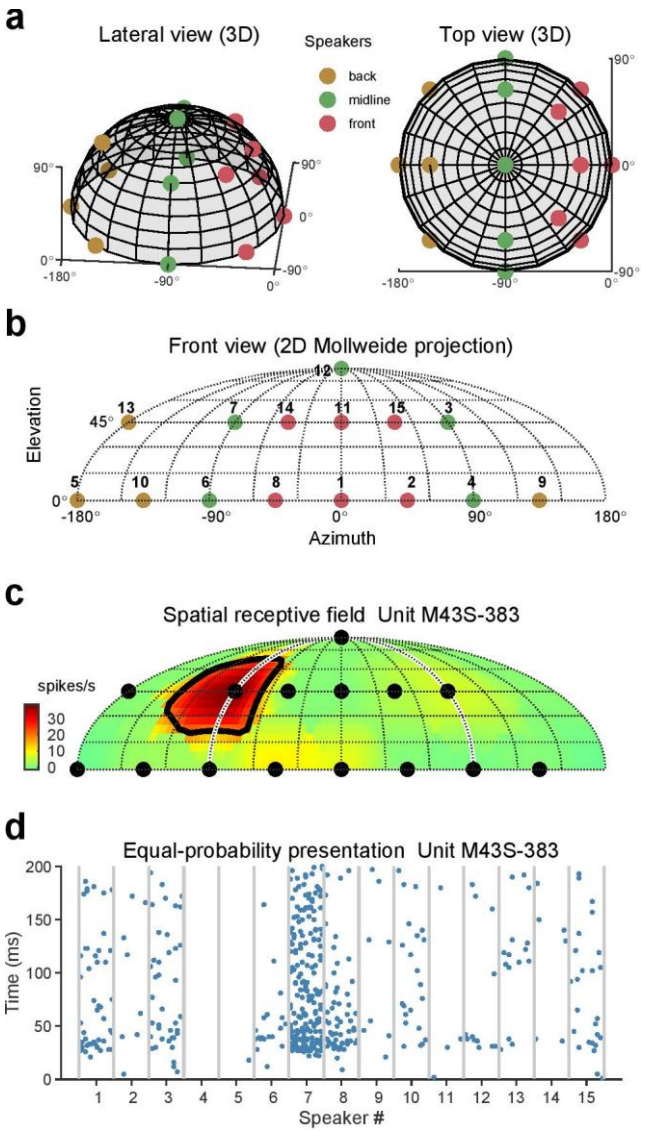

Fig. 1 Speaker layout and equal-probability sound stimulation

a, Fifteen equally spaced speakers were placed on a semi-spherical surface centered around the animal's head and above the horizontal plane. View from the front, lateral 35° and elevated 30° (left), and view from directly top (right). Red dots indicate six front speakers, green dots indicate five midline speakers, and brown dots indicate four back speakers.

b, Three-dimensional front-back space was projected to a two-dimensional plane around midline for displaying purposes.

c, Spatial receptive field of example Unit M43S-383. White semicircle is the boundary of the front-back space. Black line is the threshold which is defined as the half-maximum firing rate. Black dots indicate fifteen speaker locations.

d, Spike raster plot of same example neuron at fifteen speaker locations under equal-probability presentation mode. Stimuli at each speaker location were randomly presented ten times.

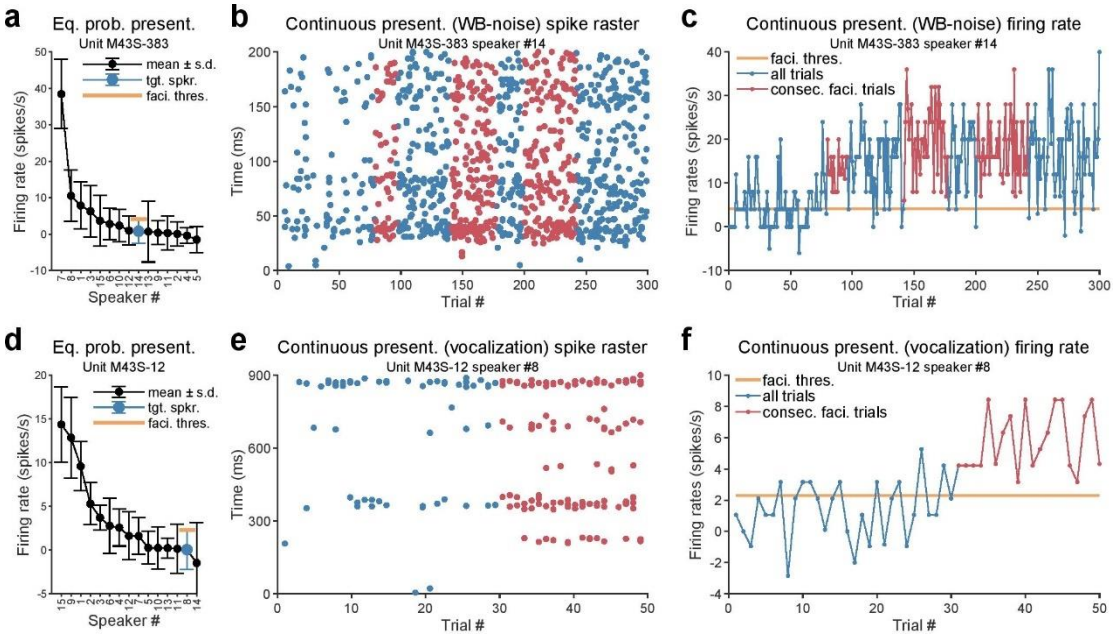

Fig. 2 Repetitive sound stimulation evoked neural facilitation

a, Firing rate versus speak number of unit M43S-383 recorded under the equal-probability presentation mode (same data as **Fig. 1d**). Blue dot and orange bar indicate the target speaker and facilitation threshold (mean + standard deviation), respectively. **b,** Spike raster of same example neuron tested at speaker #14 under continuous presentation mode. Red dots indicate spikes belong to the long facilitation phase (i.e., at least five consecutive trials with firing rates exceeding the facilitation threshold). **c,** Trial-by-trial firing rate of same example neuron. Red dots and line indicate trails belong to the long facilitation phase. Thick orange line indicates the facilitation threshold. **d-f**, Similar to **a-c**, but for Unit M43S-12 that was tested using marmoset vocalization stimuli.

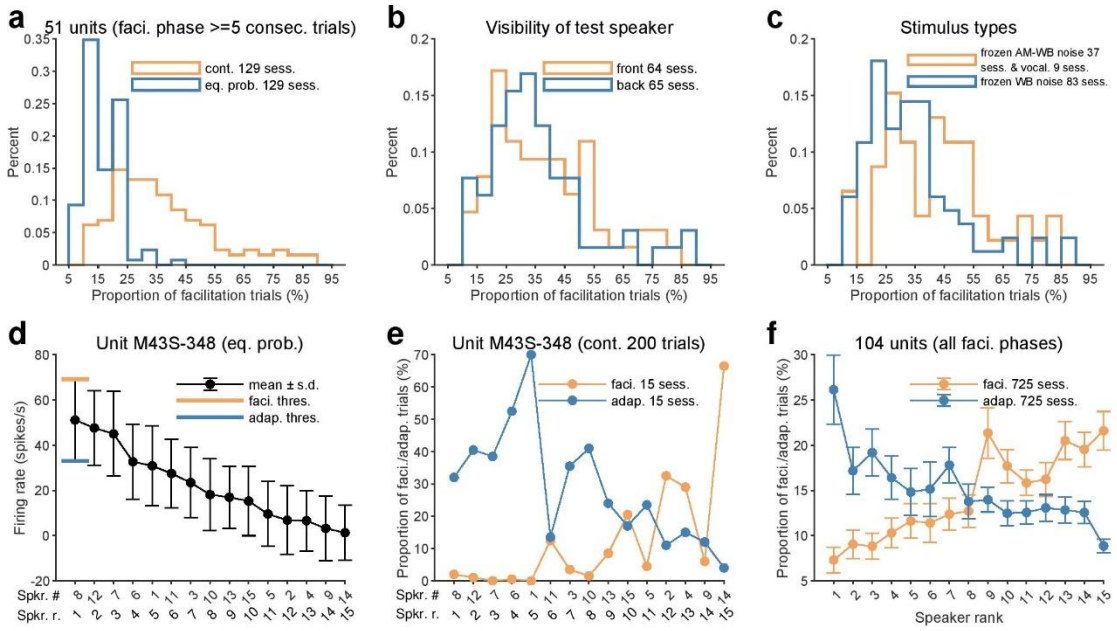

Fig. 3 Neural facilitation occurred in a variety of stimulus conditions and depends on sound locations

a, Histogram of the proportion of facilitation trials under the continuous (orange line) and equal-probability (blue line) presentation modes. Only 129 sessions from fifty-one neurons that exhibited facilitation phases lasting at least five consecutive trials were shown.

b, Histogram of the proportion of facilitation trials under the continuous presentation mode for target speakers located in the front (orange line) and back (blue line). Front speakers: #1, #2, #8, #11, #14, and #15. Back speakers: #3, #4, #5, #6, #7, #9, #10, #12, and #13.

c, Histogram of the proportion of facilitation trials under the continuous presentation mode using frozen amplitude-modulated wide-band noise or animal vocalization (orange line) and frozen unmodulated wide-band noise (blue line) as stimuli.

d, Each speaker was assigned a rank number based on its baseline firing rate obtained under the equal-probability presentation mode. Speaker ranked 1st had the highest firing rate. In this example unit M43S-348, speaker #8 ranked 1st and speaker #14 ranked 15th. Orange and blue bars indicate facilitation and adaptation threshold, respectively. Dots and error bars indicate mean ± standard deviation.

e, Proportion of facilitation (orange dots and lines) and adaptation (blue dots and lines) trials under continuous presentation mode at different speaker ranks for the same example unit. Stimuli at each speaker location were tested 200 times.

f, Proportion of facilitation (orange dots and lines) and adaptation (blue dots and lines) trials of the population data. All 725 sessions from 104 neurons were shown, regardless of the length of the facilitation phase.

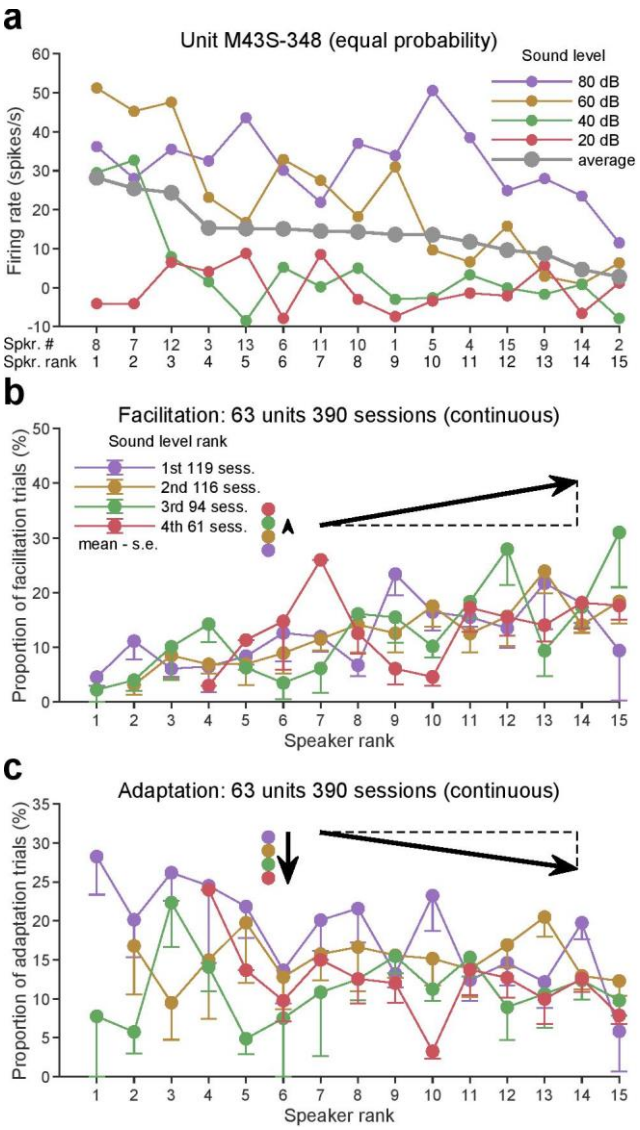

Fig. 4 Neural facilitation primarily depends on sound location but not firing rate

a, Example unit M43S-348's averaged responses to wide-band noise played at four sound levels across fifteen speaker locations (violet/brown/green/red dots and lines). Speaker rank was determined by the averaged firing rate at four sound levels (black dots and line).

b, Proportion of facilitation trials at fifteen speaker ranks (same color dots and lines in x-axis) and four sound level ranks (different color dots and bars in y-axis) were assigned based on the response obtained under the equal-probability mode. Length of upwards arrow is proportional to the proportion of facilitation trials averaged across speakers. Slope of the northeast arrow is proportional to the proportion of facilitation trials averaged across sound levels. Dots and error bars indicate mean - standard deviation of mean.

c, Similar to **b**, but for adaptation. Length of the downwards arrow is proportional to the proportion of adaptation trials averaged across speakers. Slope of the southeast arrow is proportional to the proportion of adaptation trials averaged across sound levels.

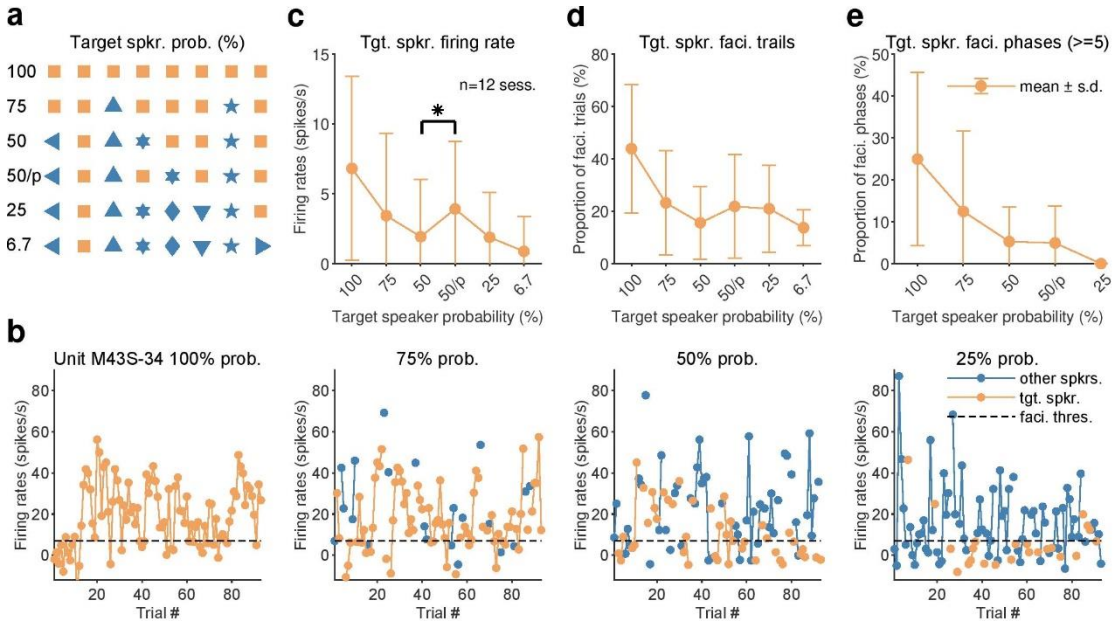

Fig. 5 Dependence of neural facilitation on location continuity

a, Six stimulus presentation modes were used in our studies. Continuous presentation mode equals to 100% probability presentation mode. 75%, 50% and 25% probabilistic presentation modes play sounds from all fifteen speakers in a randomly shuffled order, while giving the target speaker (orange square) a presentation probability higher than other speakers (blue left-pointing triangle, upward-pointing triangle, hexagram, diamond, downward-pointing triangle, pentagram, right-pointing triangle). For the 50% probability periodic presentation mode (50/p%), the target speaker was interleaved with other speakers. Therefore, the sequence of the target speaker was periodic instead of random. Equal-probability presentation mode equals to 6.7% probability presentation mode.

b, Firing rate of target speaker (orange dots and lines) and other speakers (blue dots and lines) for example unit M43S-34 under 100% (left), 75% (middle-left), 50% (middle-right), and 25% (right) probability presentation modes. Black dashed line indicates the facilitation threshold.

c, Firing rate of target speaker for six presentation modes. *, $p<0.05$, rank-sum test. Dots and error bars indicate mean ± standard deviation.

d, Proportion of facilitation trials that belong to all facilitation phases at target speaker.

e, Proportion of facilitation trials that belong to facilitation phases that lasting at least five consecutive trials at target speaker.

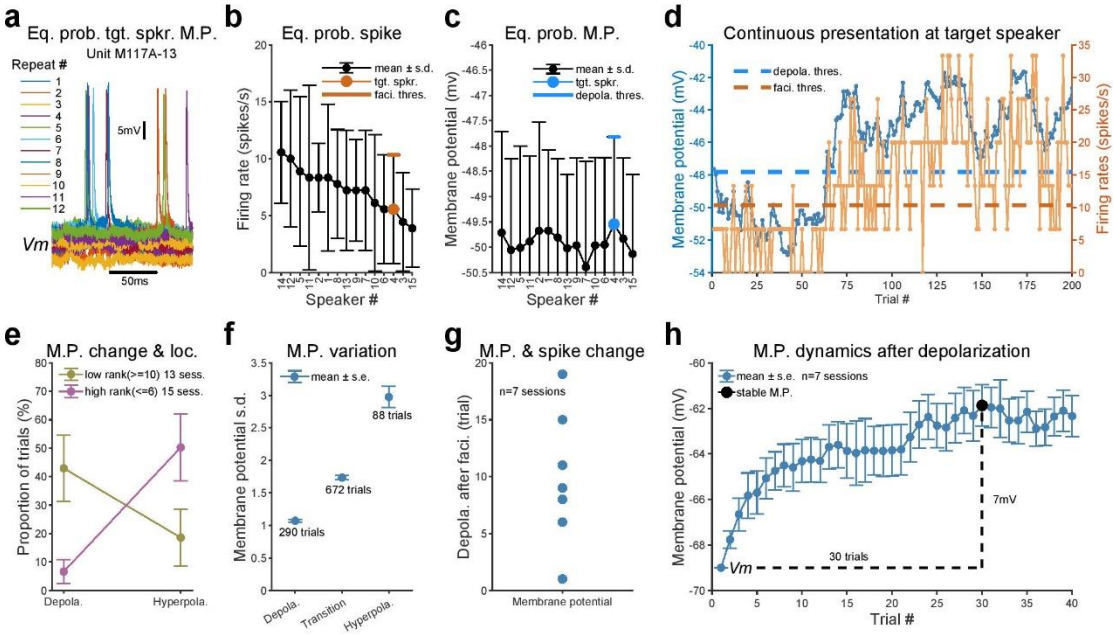

Fig. 6 Repetitive sound stimulation induced sustained membrane potential depolarization

a, Membrane potential traces of unit M117A-13 recorded under the equal-probability presentation mode at the target speaker location. Each color line indicates one trial.

b, Firing rate based speaker rank of same neuron obtained under the equal-probability presentation mode. Orange dot and bar indicate the target speaker and its facilitation threshold.

c, Corresponding membrane potential (spikes removed) at the same speaker rank used in **b**. Blue dot and bar indicate the target speaker and its depolarization threshold.

d, Membrane potential (blue line and dots) and total firing rate (i.e., not minus the spontaneous firing rate, orange line and dots) changes during the continuous presentation mode. Threshold of facilitation (dashed orange line) and depolarization (dashed blue line) were calculated in **b** and **c**, respectively.

e, Target speakers were divided into a low ranked group (10th to 15th, gold dots and bars) and a high ranked group (1st to 6th, violet dots and bars). Dots and error bars indicate mean ± standard deviation of mean.

f, The standard deviation of membrane potential for depolarization, transition and hyperpolarization trials across all sessions.

g, Number of trials needed to achieve the first membrane potential depolarization phase and the spiking facilitation phase that both lasting at least five consecutive trials.

h, Changes in membrane potential magnitude after depolarization (blue dots and line). Black dot indicates the stabilized membrane potential.

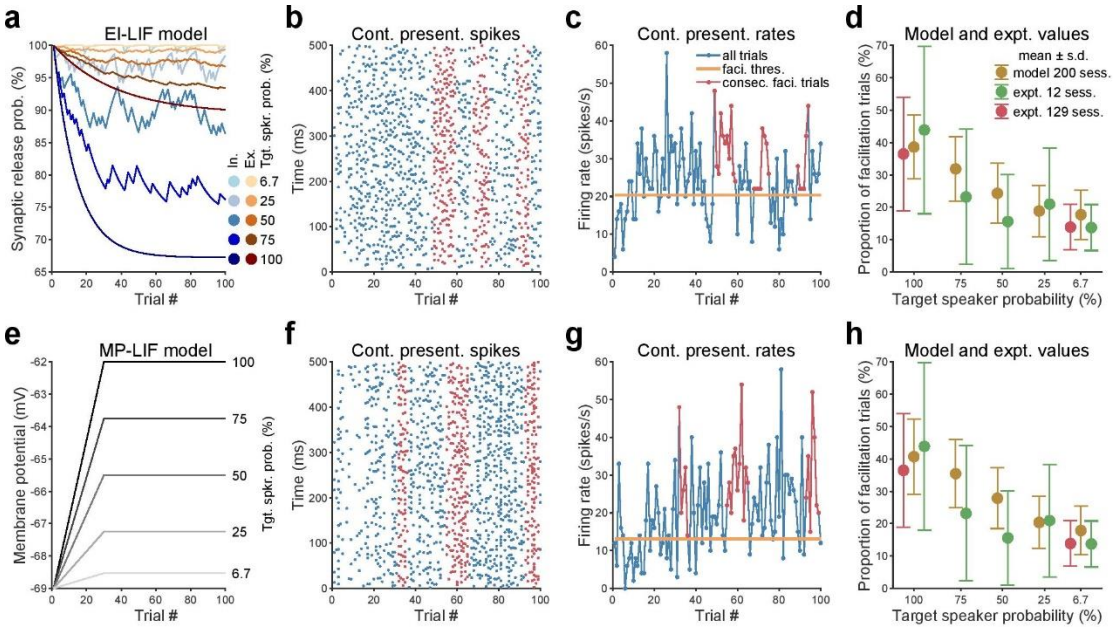

Fig. 7 Computational models suggest two distinct neural mechanisms underlying location-specific facilitation

a, Inhibitory (blue lines and dots) and excitatory (orange lines and dots) synaptic depression leaky integrate-and-fire model (EI-LIF model). Under the continuous presentation mode, synaptic release probability at five probability presentation modes decreased gradually.

b, Spike raster plot for one session of EI-model neuron during continuous sound presentation mode. Red dots indicate spikes belong to long facilitation phase (i.e., at least five consecutive trials with firing rates exceeding the facilitation threshold).

c, Trial-by-trial firing rate from the same session of EI-model neuron. Red dots and line indicate trails belong to the long facilitation phase. Thick orange line indicates the facilitation threshold (i.e., one standard deviation above the baseline firing rate).

d, Decrease the presentation probability of target speaker resulted in a smaller proportion of facilitation trials for 200 sessions of EI-LIF model neuron (brown dots and bars). Green dots and bars show the data from five probability presentation modes (twelve sessions, same as Fig. 5d). Red dots and bars show the data from continuous and equal-probability presentation modes (129 sessions, same as Fig. 3a). Dots and error bars indicate mean ± standard deviation.

e-h, Similar to **a-d** but for membrane potential depolarization leaky integrate-and-fire model (MP-LIF model).

References

1. Andreou, L.V., Kashino, M. & Chait, M. The role of temporal regularity in auditory segregation. *Hear Res* **280**, 228-235 (2011).
2. Asari, H. & Zador, A.M. Long-lasting context dependence constrains neural encoding models in rodent auditory cortex. *J Neurophysiol* **102**, 2638-2656 (2009).
3. Auksztulewicz, R.*, et al.* The Cumulative Effects of Predictability on Synaptic Gain in the Auditory Processing Stream. *J Neurosci* **37**, 6751-6760 (2017).
4. Awwad, B., Jankowski, M.M. & Nelken, I. Synaptic Recruitment Enhances Gap Termination Responses in Auditory Cortex. *Cereb Cortex* **30**, 4465-4480 (2020).
5. Barascud, N., Pearce, M.T., Griffiths, T.D., Friston, K.J. & Chait, M. Brain responses in humans reveal ideal observer-like sensitivity to complex acoustic patterns. *Proc Natl Acad Sci U S A* **113**, E616-625 (2016).
6. Bartlett, E.L. & Wang, X. Long-lasting modulation by stimulus context in primate auditory cortex. *J Neurophysiol* **94**, 83-104 (2005).
7. Bendixen, A., Denham, S.L., Gyimesi, K. & Winkler, I. Regular patterns stabilize auditory streams. *J Acoust Soc Am* **128**, 3658-3666 (2010).
8. Brosch, M. & Scheich, H. Tone-sequence analysis in the auditory cortex of awake macaque monkeys. *Exp Brain Res* **184**, 349-361 (2008).
9. Brosch, M. & Schreiner, C.E. Sequence sensitivity of neurons in cat primary auditory cortex. *Cereb Cortex* **10**, 1155-1167 (2000).
10. Brosch, M., Schulz, A. & Scheich, H. Processing of sound sequences in macaque auditory cortex: response enhancement. *J Neurophysiol* **82**, 1542-1559 (1999).
11. Calford, M.B. & Semple, M.N. Monaural inhibition in cat auditory cortex. *J Neurophysiol* **73**, 1876-1891 (1995).
12. Carbajal, G.V. & Malmierca, M.S. The Neuronal Basis of Predictive Coding Along the Auditory Pathway: From the Subcortical Roots to Cortical Deviance Detection. *Trends Hear* **22**, 2331216518784822 (2018).
13. Chadderton, P., Agapiou, J.P., McAlpine, D. & Margrie, T.W. The synaptic representation of sound source location in auditory cortex. *J Neurosci* **29**, 14127-14135 (2009).
14. Chaplin, T.A., Yu, H.H. & Rosa, M.G. Representation of the visual field in the primary visual area of the marmoset monkey: magnification factors, point-image size, and proportionality to retinal ganglion cell density. *J Comp Neurol* **521**, 1001-1019 (2013).
15. Chen, I.W., Helmchen, F. & Lutcke, H. Specific Early and Late Oddball-Evoked Responses in Excitatory and Inhibitory Neurons of Mouse Auditory Cortex. *J Neurosci* **35**, 12560-12573 (2015).
16. Cherry, E.C. Some experiments on the Recognition of Speech with one or two ears. *J Acoust Soc Am* (1953).
17. Condon, C.D. & Weinberger, N.M. Habituation produces frequency-specific plasticity of receptive fields in the auditory cortex. *Behav Neurosci* **105**, 416-430 (1991).
18. Dragoi, V., Sharma, J. & Sur, M. Adaptation-induced plasticity of orientation tuning in adult visual cortex. *Neuron* **28**, 287-298 (2000).
19. Farley, B.J., Quirk, M.C., Doherty, J.J. & Christian, E.P. Stimulus-specific adaptation in auditory cortex is an NMDA-independent process distinct from the sensory novelty encoded by

the mismatch negativity. *J Neurosci* **30**, 16475-16484 (2010).
20. Feng, L. & Wang, X. Harmonic template neurons in primate auditory cortex underlying complex sound processing. *Proc Natl Acad Sci U S A* **114**, E840-E848 (2017).
21. Fishman, Y.I. & Steinschneider, M. Searching for the mismatch negativity in primary auditory cortex of the awake monkey: deviance detection or stimulus specific adaptation? *J Neurosci* **32**, 15747-15758 (2012).
22. Fitzpatrick, D.C., Kuwada, S., Kim, D.O., Parham, K. & Batra, R. Responses of neurons to click-pairs as simulated echoes: auditory nerve to auditory cortex. *J Acoust Soc Am* **106**, 3460-3472 (1999).
23. Galarreta, M. & Hestrin, S. Frequency-dependent synaptic depression and the balance of excitation and inhibition in the neocortex. *Nat Neurosci* **1**, 587-594 (1998).
24. Gao, L., Kostlan, K., Wang, Y. & Wang, X. Distinct Subthreshold Mechanisms Underlying Rate-Coding Principles in Primate Auditory Cortex. *Neuron* **91**, 905-919 (2016).
25. Gao, L. & Wang, X. Subthreshold Activity Underlying the Diversity and Selectivity of the Primary Auditory Cortex Studied by Intracellular Recordings in Awake Marmosets. *Cereb Cortex* **29**, 994-1005 (2019).
26. Harpaz, M., Jankowski, M.M., Khouri, L. & Nelken, I. Emergence of abstract sound representations in the ascending auditory system. *Prog Neurobiol* **202**, 102049 (2021).
27. Heiss, J.E., Katz, Y., Ganmor, E. & Lampl, I. Shift in the balance between excitation and inhibition during sensory adaptation of S1 neurons. *J Neurosci* **28**, 13320-13330 (2008).
28. Hershenhoren, I., Taaseh, N., Antunes, F.M. & Nelken, I. Intracellular correlates of stimulus-specific adaptation. *J Neurosci* **34**, 3303-3319 (2014).
29. Huang, N. & Elhilali, M. Push-pull competition between bottom-up and top-down auditory attention to natural soundscapes. *Elife* **9** (2020).
30. Kato, H.K., Gillet, S.N. & Isaacson, J.S. Flexible Sensory Representations in Auditory Cortex Driven by Behavioral Relevance. *Neuron* **88**, 1027-1039 (2015).
31. Kayser, C., Petkov, C.I., Lippert, M. & Logothetis, N.K. Mechanisms for allocating auditory attention: an auditory saliency map. *Curr Biol* **15**, 1943-1947 (2005).
32. Keating, P., Dahmen, J.C. & King, A.J. Complementary adaptive processes contribute to the developmental plasticity of spatial hearing. *Nat Neurosci* **18**, 185-187 (2015).
33. Kilgard, M.P. & Merzenich, M.M. Order-sensitive plasticity in adult primary auditory cortex. *Proc Natl Acad Sci U S A* **99**, 3205-3209 (2002).
34. Kommajosyula, S.P., Bartlett, E.L., Cai, R., Ling, L. & Caspary, D.M. Corticothalamic projections deliver enhanced responses to medial geniculate body as a function of the temporal reliability of the stimulus. *J Physiol* **599**, 5465-5484 (2021).
35. Kuchibhotla, K.V*., et al.* Parallel processing by cortical inhibition enables context-dependent behavior. *Nat Neurosci* **20**, 62-71 (2017).
36. Kyweriga, M., Stewart, W., Cahill, C. & Wehr, M. Synaptic mechanisms underlying interaural level difference selectivity in rat auditory cortex. *J Neurophysiol* **112**, 2561-2571 (2014).
37. Lee, C.C. & Middlebrooks, J.C. Auditory cortex spatial sensitivity sharpens during task performance. *Nat Neurosci* **14**, 108-114 (2011).
38. Lesicko, A.M.H., Angeloni, C.F., Blackwell, J.M., De Biasi, M. & Geffen, M.N. Corticofugal regulation of predictive coding. *Elife* **11** (2022).

39. Luck, S.J., Chelazzi, L., Hillyard, S.A. & Desimone, R. Neural mechanisms of spatial selective attention in areas V1, V2, and V4 of macaque visual cortex. *J Neurophysiol* **77**, 24-42 (1997).
40. Malmierca, M.S. & Auksztulewicz, R. Stimulus-specific adaptation, MMN and predictive coding. *Hear Res* **399**, 108076 (2021).
41. Malmierca, M.S., Sanchez-Vives, M.V., Escera, C. & Bendixen, A. Neuronal adaptation, novelty detection and regularity encoding in audition. *Front Syst Neurosci* **8**, 111 (2014).
42. Malone, B.J., Scott, B.H. & Semple, M.N. Context-dependent adaptive coding of interaural phase disparity in the auditory cortex of awake macaques. *J Neurosci* **22**, 4625-4638 (2002).
43. Masutomi, K., Barascud, N., Kashino, M., McDermott, J.H. & Chait, M. Sound segregation via embedded repetition is robust to inattention. *J Exp Psychol Hum Percept Perform* **42**, 386-400 (2016).
44. McDermott, J.H. The cocktail party problem. *Curr Biol* **19**, R1024-1027 (2009).
45. McDermott, J.H., Wrobleski, D. & Oxenham, A.J. Recovering sound sources from embedded repetition. *Proc Natl Acad Sci U S A* **108**, 1188-1193 (2011).
46. McGinley, M.J., David, S.V. & McCormick, D.A. Cortical Membrane Potential Signature of Optimal States for Sensory Signal Detection. *Neuron* **87**, 179-192 (2015).
47. Mickey, B.J. & Middlebrooks, J.C. Representation of auditory space by cortical neurons in awake cats. *J Neurosci* **23**, 8649-8663 (2003).
48. Mickey, B.J. & Middlebrooks, J.C. Sensitivity of auditory cortical neurons to the locations of leading and lagging sounds. *J Neurophysiol* **94**, 979-989 (2005).
49. Middlebrooks, J.C. & Pettigrew, J.D. Functional classes of neurons in primary auditory cortex of the cat distinguished by sensitivity to sound location. *J Neurosci* **1**, 107-120 (1981).
50. Mitchell, J.F., Sundberg, K.A. & Reynolds, J.H. Differential attention-dependent response modulation across cell classes in macaque visual area V4. *Neuron* **55**, 131-141 (2007).
51. Mrsic-Flogel, T.D., King, A.J. & Schnupp, J.W. Encoding of virtual acoustic space stimuli by neurons in ferret primary auditory cortex. *J Neurophysiol* **93**, 3489-3503 (2005).
52. Naatanen, R., Paavilainen, P., Rinne, T. & Alho, K. The mismatch negativity (MMN) in basic research of central auditory processing: a review. *Clin Neurophysiol* **118**, 2544-2590 (2007).
53. Natan, R.G.*, et al.* Complementary control of sensory adaptation by two types of cortical interneurons. *Elife* **4** (2015).
54. Natan, R.G., Rao, W. & Geffen, M.N. Cortical Interneurons Differentially Shape Frequency Tuning following Adaptation. *Cell Rep* **21**, 878-890 (2017).
55. Nelken, I. Stimulus-specific adaptation and deviance detection in the auditory system: experiments and models. *Biol Cybern* **108**, 655-663 (2014).
56. Nelken, I., Prut, Y., Vaddia, E. & Abeles, M. Population responses to multifrequency sounds in the cat auditory cortex: four-tone complexes. *Hear Res* **72**, 223-236 (1994).
57. Nelken, I., Yaron, A., Polterovich, A. & Hershenhoren, I. Stimulus-specific adaptation beyond pure tones. *Adv Exp Med Biol* **787**, 411-418 (2013).
58. Nieto-Diego, J. & Malmierca, M.S. Topographic Distribution of Stimulus-Specific Adaptation across Auditory Cortical Fields in the Anesthetized Rat. *PLoS Biol* **14**, e1002397 (2016).
59. O'Neill, W.E. & Suga, N. Target range-sensitive neurons in the auditory cortex of the mustache bat. *Science* **203**, 69-73 (1979).

60. Parras, G.G., *et al.* Neurons along the auditory pathway exhibit a hierarchical organization of prediction error. *Nat Commun* **8**, 2148 (2017).
61. Perez-Gonzalez, D., *et al.* Deviance detection in physiologically identified cell types in the rat auditory cortex. *Hear Res* **399**, 107997 (2021).
62. Phillips, E.A.K., Schreiner, C.E. & Hasenstaub, A.R. Diverse effects of stimulus history in waking mouse auditory cortex. *J Neurophysiol* **118**, 1376-1393 (2017).
63. Polterovich, A., Jankowski, M.M. & Nelken, I. Deviance sensitivity in the auditory cortex of freely moving rats. *PLoS One* **13**, e0197678 (2018).
64. Popescu, M.V. & Polley, D.B. Monaural deprivation disrupts development of binaural selectivity in auditory midbrain and cortex. *Neuron* **65**, 718-731 (2010).
65. Reale, R.A. & Brugge, J.F. Directional sensitivity of neurons in the primary auditory (AI) cortex of the cat to successive sounds ordered in time and space. *J Neurophysiol* **84**, 435-450 (2000).
66. Remington, E.D. & Wang, X. Neural Representations of the Full Spatial Field in Auditory Cortex of Awake Marmoset (Callithrix jacchus). *Cereb Cortex* **29**, 1199-1216 (2019).
67. Reynolds, J.H., Pasternak, T. & Desimone, R. Attention increases sensitivity of V4 neurons. *Neuron* **26**, 703-714 (2000).
68. Sadagopan, S. & Wang, X. Level invariant representation of sounds by populations of neurons in primary auditory cortex. *J Neurosci* **28**, 3415-3426 (2008).
69. Sadagopan, S. & Wang, X. Nonlinear spectrotemporal interactions underlying selectivity for complex sounds in auditory cortex. *J Neurosci* **29**, 11192-11202 (2009).
70. Scholes, C., Palmer, A.R. & Sumner, C.J. Forward suppression in the auditory cortex is frequency-specific. *Eur J Neurosci* **33**, 1240-1251 (2011).
71. Shamma, S.A. & Micheyl, C. Behind the scenes of auditory perception. *Curr Opin Neurobiol* **20**, 361-366 (2010).
72. Southwell, R., *et al.* Is predictability salient? A study of attentional capture by auditory patterns. *Philos Trans R Soc Lond B Biol Sci* **372** (2017).
73. Suga, N., O'Neill, W.E. & Manabe, T. Harmonic-sensitive neurons in the auditory cortex of the mustache bat. *Science* **203**, 270-274 (1979).
74. Sutter, M.L. & Schreiner, C.E. Physiology and topography of neurons with multipeaked tuning curves in cat primary auditory cortex. *J Neurophysiol* **65**, 1207-1226 (1991).
75. Thomas, J.M., *et al.* Stimulus-specific adaptation in specialized neurons in the inferior colliculus of the big brown bat, Eptesicus fuscus. *Hear Res* **291**, 34-40 (2012).
76. Torrado Pacheco, A., *et al.* Rapid and active stabilization of visual cortical firing rates across light-dark transitions. *Proc Natl Acad Sci U S A* **116**, 18068-18077 (2019).
77. Ulanovsky, N., Las, L., Farkas, D. & Nelken, I. Multiple time scales of adaptation in auditory cortex neurons. *J Neurosci* **24**, 10440-10453 (2004).
78. Ulanovsky, N., Las, L. & Nelken, I. Processing of low-probability sounds by cortical neurons. *Nat Neurosci* **6**, 391-398 (2003).
79. van der Heijden, K., Rauschecker, J.P., Formisano, E., Valente, G. & de Gelder, B. Active Sound Localization Sharpens Spatial Tuning in Human Primary Auditory Cortex. *J Neurosci* **38**, 8574-8587 (2018).
80. Wang, C.A., Boehnke, S.E., Itti, L. & Munoz, D.P. Transient pupil response is modulated by contrast-based saliency. *J Neurosci* **34**, 408-417 (2014).

81. Wang, X. Cortical Coding of Auditory Features. *Annu Rev Neurosci* **41**, 527-552 (2018).
82. Wehr, M. & Zador, A.M. Synaptic mechanisms of forward suppression in rat auditory cortex. *Neuron* **47**, 437-445 (2005).
83. Woods, T.M., Lopez, S.E., Long, J.H., Rahman, J.E. & Recanzone, G.H. Effects of stimulus azimuth and intensity on the single-neuron activity in the auditory cortex of the alert macaque monkey. *J Neurophysiol* **96**, 3323-3337 (2006).
84. Yan, Y., Zhaoping, L. & Li, W. Bottom-up saliency and top-down learning in the primary visual cortex of monkeys. *Proc Natl Acad Sci U S A* **115**, 10499-10504 (2018).
85. Yaron, A., Hershenhoren, I. & Nelken, I. Sensitivity to complex statistical regularities in rat auditory cortex. *Neuron* **76**, 603-615 (2012).
86. Zhou, Y. & Wang, X. Level dependence of spatial processing in the primate auditory cortex. *J Neurophysiol* **108**, 810-826 (2012).
87. Zhou, Y. & Wang, X. Spatially extended forward suppression in primate auditory cortex. *Eur J Neurosci* **39**, 919-933 (2014).

Acknowledgements

This research was supported by National Institute of Health grants DC003180 and DC005808 to X.W. We thank A. Pistorio, and J. Estes for assistance with animal care, X. Song, X. Liu, and H. Mandal for their comments on the earlier versions of the manuscript.

Competing interests

The authors declare no completing interests.

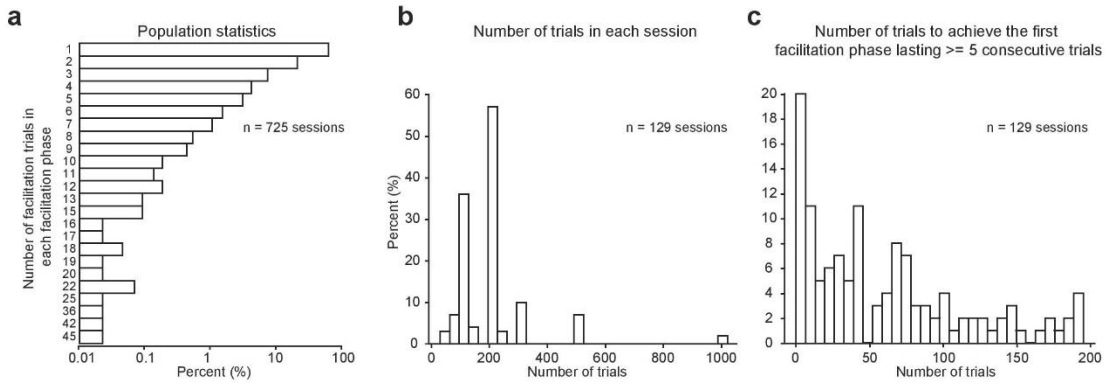

Extended Data Fig. 1 Population statistics

a, Logarithmic histogram of the number of facilitated trials in each facilitation phase. We chose the sessions that exhibited facilitation phases lasting at least five consecutive trials as the threshold. Fifty-one neurons passed the threshold.

b, Histogram of the proportion of tested trials in each session (fifty-one neurons).

c, Histogram of the proportion of trials that was required to achieve the first facilitation phase lasting at least five consecutive trials (fifty-one neurons).

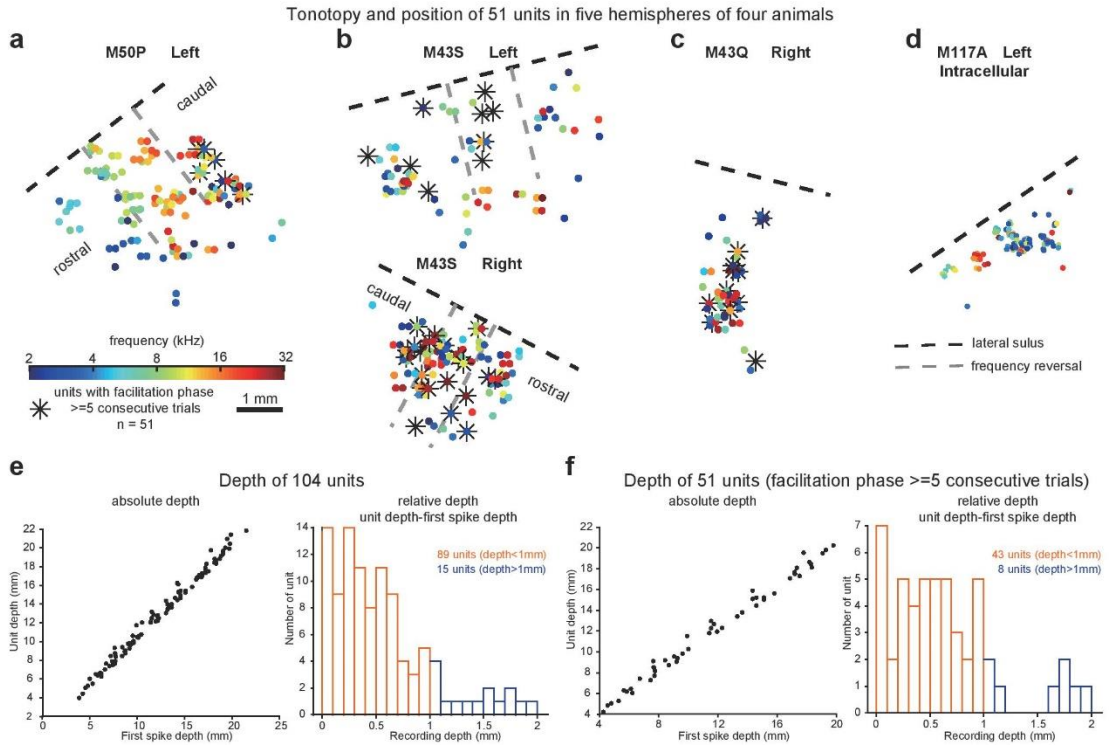

Extended Data Fig. 2 Facilitation neurons across cortical areas and layers

a-d, Best frequency (BF) distribution on the cortical surface from five hemispheres of four monkeys. The BF of recorded neurons (color dots) was examined based on their responses to pure tones stimuli ranging from 2kHz (blue) to 32kHz (red). Fifty-one neurons that exhibited facilitation phases lasting at least five consecutive trials were labeled with asterisks. The black dashed line marked the lateral sulcus line approximated by the bone suture in the temporal lobe. The auditory cortex was divided (gray dashed line) into the rostral primary auditory cortex (A1), caudal A1, and caudal area (caudal lateral and caudal medial) along the rostral-caudal axis based on the BF distribution change. **a**, Tonotopy from left hemisphere of Monkey 1. Six facilitated neurons were located in caudal area. **b**, Ten facilitated neurons (two overlapped) located in A1 of left hemisphere (top) and twenty-two facilitated neurons (two overlapped) located in A1 and caudal area of right hemisphere (bottom) of Monkey 2. **c**, Thirteen facilitated neurons (two overlapped) from right hemisphere of Monkey 3. **d**, Fourteen neurons were recorded using the intracellular recording method in the left hemisphere of Monkey 4.
e, Depth information for all the 104 neurons. Left, first spike depth (x-axis) is the absolute depth where the first spike is detected, unit depth (y-axis) is the absolute depth where the neuron is recorded currently. Right, recording depth equals to the relative depth which is calculated as the unit depth minus first spike depth. Eighty-nine neurons came from supragranular layers (recording depth less than 1mm, orange bars).
f, Same to **e** but for fifty-one neurons that exhibited facilitation phases lasting at least five consecutive trials. Forty-three neurons came from supragranular layers (orange bars).

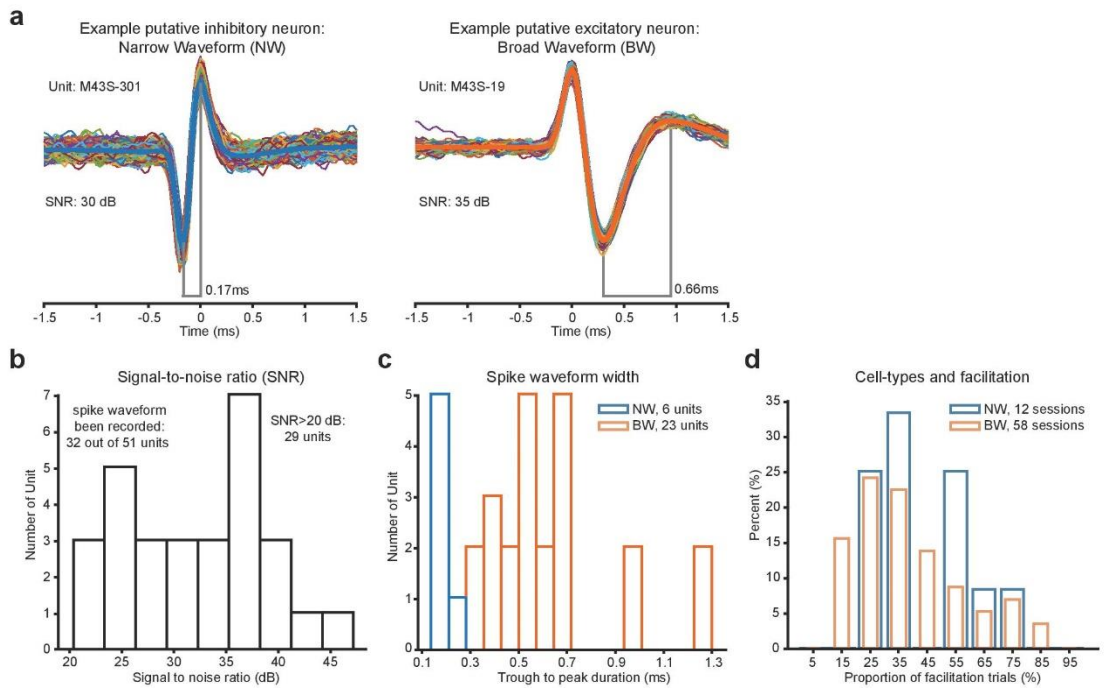

Extended Data Fig. 3 Facilitation in putative excitatory and inhibitory neurons

a, Example putative inhibitory narrow-waveform (NW, left) and putative excitatory broad-waveform (BW, right) neurons.

b, Among the fifty-one neurons with facilitation phase lasting at least five consecutive trials, the waveform of thirty-two neurons has been recorded. Twenty-nine neurons have a signal-to-noise ratio that was larger than 20dB.

c, Among the twenty-nine neurons, we used 0.3ms trough to peak duration as the boundary for classifying putative inhibitory (blue bars) and excitatory (orange bars) neurons. 21% of neurons were classified as putative inhibitory neurons.

d, Histogram of the proportion of facilitation trials between putative inhibitory (blue bars) and excitatory (orange bars) neurons.

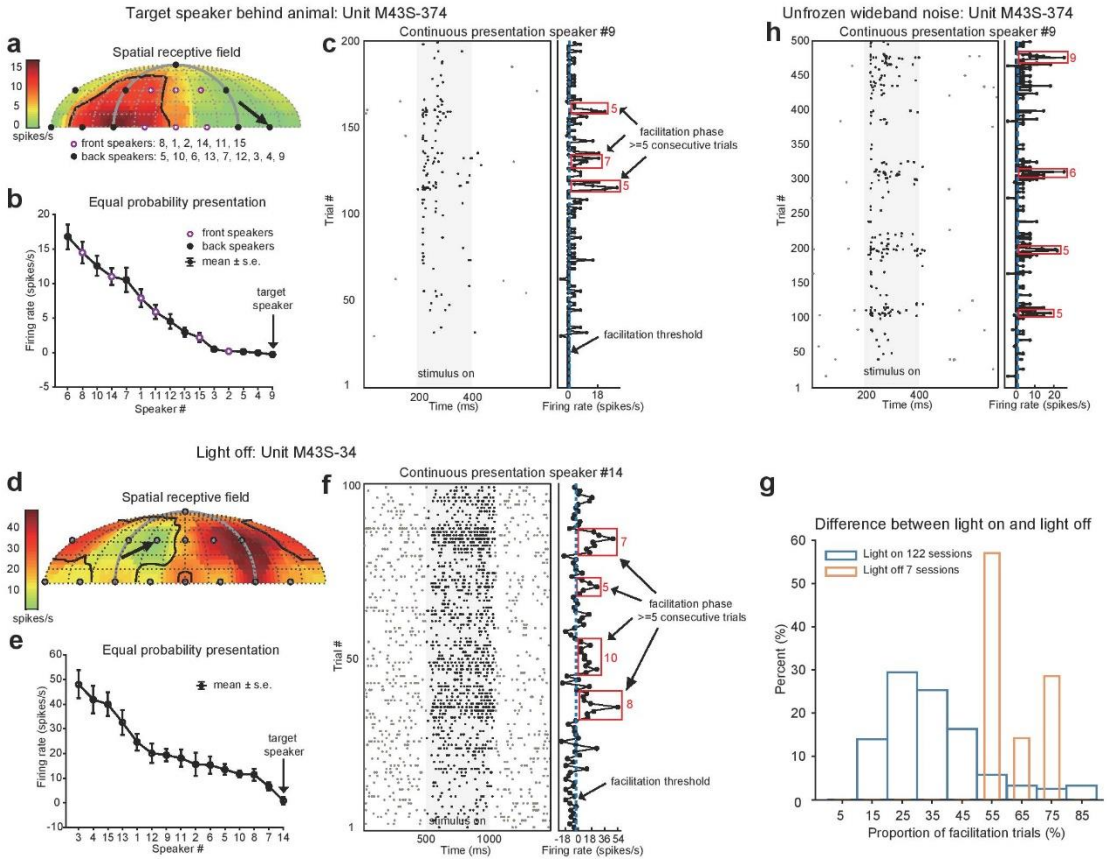

Extended Data Fig. 4 Facilitation occurred in the back, in the darkness, in using unfrozen wideband noises

a, Spatial receptive field of example unit M43S-374 obtained under equal-probability presentation mode. Black arrow indicates the spatial location of continuously presented stimuli. Six orange circles indicate front speakers, and nine black dots indicate back speakers.

b, Firing rate versus speak number of same example neuron under the equal-probability presentation mode.

c, Left, spike raster of same example neuron tested at speaker #9 under continuous sound presentation mode. Gray shaded area indicates the sound presentation period. Right, trial-by-trial firing rate. Dashed blue line indicates the facilitation threshold. Red squares include trials belonging to the long facilitation phase (i.e., at least five consecutive trials with firing rates exceeding the facilitation threshold).

d-f, Similar to **a-c**, but the example unit M43S-34 was tested under the light-off condition.

g, Histogram of the proportion of facilitation trials under the continuous presentation mode for light on (blue bars) and off (orange bars) sessions. Among the seven light-off sessions, five sessions were tested when light was turned off, and two sessions were tested when both eyes were blocked by an acoustic drape.

h, Unfrozen wideband noise stimuli were tested for example unit M43S-374. Four sessions tested with unfrozen wideband noise stimuli were not included in 129 sessions mentioned above.

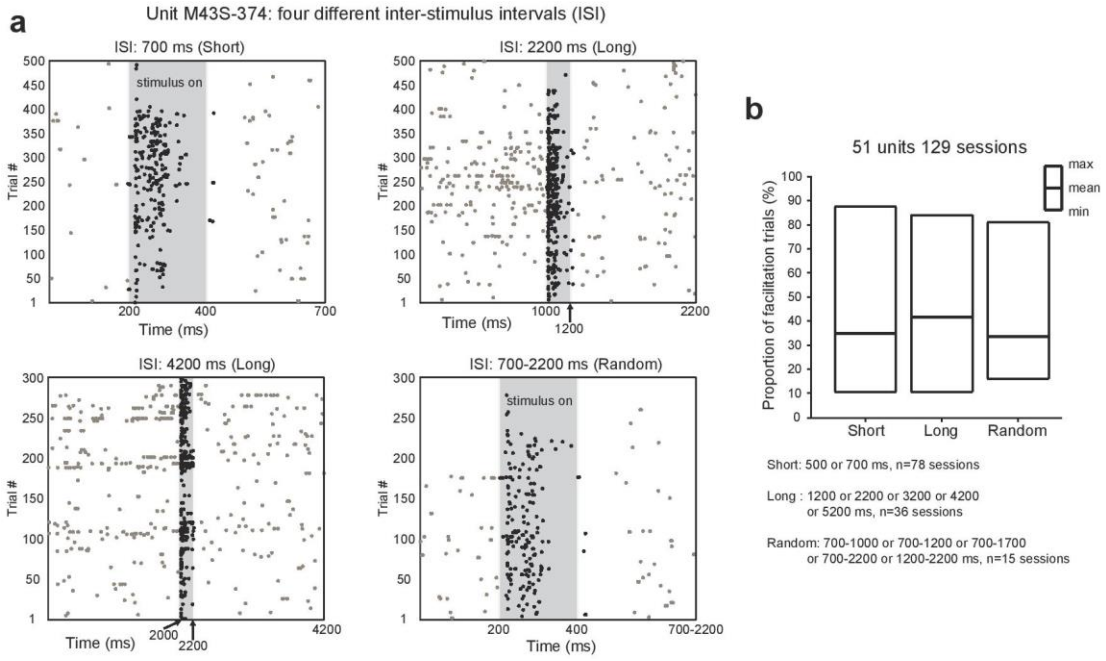

Extended Data Fig. 5 Facilitation occurred using different ISIs

a, Example unit M43S-374 showed neural facilitation at fixed length 700ms ISI (top left), 2200ms ISI (top right), 4200ms ISI (bottom left), and random length 700-2200ms ISI (bottom right). Gray shaded area indicates the sound presentation period.

b, Across the 129 sessions with facilitation phase lasting at least five consecutive trials, ISIs were classified into three groups: short (500 and 700ms, 78 sessions), long (1200, 2200, 3200, 4200 and 5200ms, 36 sessions) and random (700-1000 or 700-1200 or 700-1700 or 700-2200 or 1200-2200ms, 15 sessions).

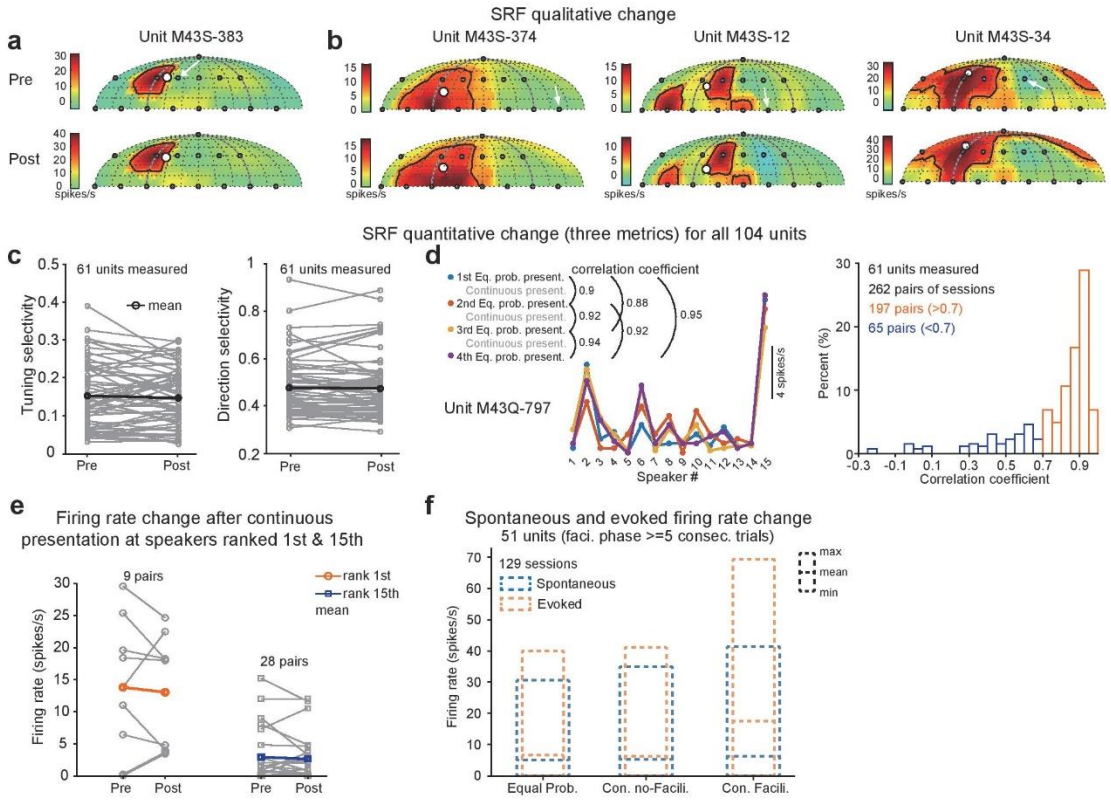

Extended Data Fig. 6 Neural facilitation did not alter SRF

a, Spatial receptive field under the equal-probability presentation mode before (up) and after (down) the presentation of continuous sound stimuli (same neuron in **Fig. 1c**). White arrow indicates the speaker location tested under continuous presentation mode. Area within the enclosed black line is proportional to the reciprocal of tuning selectivity, and the size of white dot is proportional to the direction selectivity.

b, Similar to **a** but for all other three example neurons.

c, Tuning selectivity (left) and direction selectivity (right) before and after the continuous presentation mode.

d, Left, the pairwise correlation coefficient between each pair of responses to fifteen speaker locations in the example unit M43Q-797. Color dots and lines indicate averaged firing rate under equal-probability presentation modes. Right, histogram of the correlation coefficient before and after the continuous presentation mode. Orange bars indicate paired sessions with a correlation coefficient greater larger than 0.7.

e, Total firing rates (i.e., without minus the spontaneous firing rate) changes for the highest (1st, orange circles and line) and lowest (15th, blue circles and line) ranked target speakers (rank 1st: p = 0.7962, rank 15th: p = 0.9738, rank-sum test). Color dots indicate the mean value.

f, Spontaneous (blue dashed boxes) and evoked (orange dashed boxes) total firing rates of equal-probability presentation mode, non-facilitation, and facilitation phases of the continuous presentation mode. For equal-probability presentation mode, only trials using the target speaker were included.

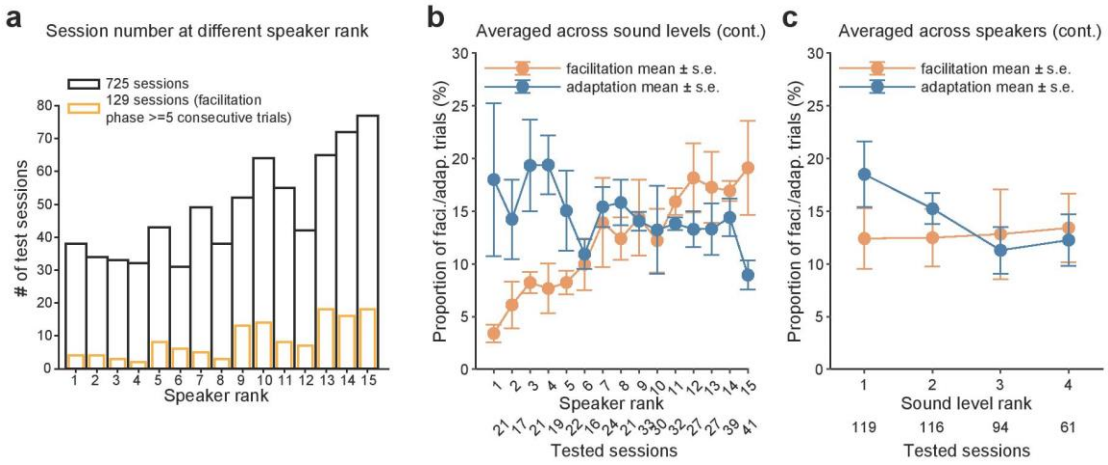

Extended Data Fig. 7 Proportion of facilitation and adaptation trials averaged across sound levels and speakers

a, Number of all tested sessions (black bars) and sessions with facilitation phases lasting at least five consecutive trials (yellow bars) at different speaker rank.

b, Proportion of facilitation (orange dots and bars) and adaptation (blue dots and bars) trials averaged across sound levels under the continuous presentation mode. Dots and error bars indicate mean ± standard deviation of mean.

c, Proportion of facilitation (orange dots and bars) and adaptation (blue dots and bars) trials averaged across speakers under the continuous presentation mode.

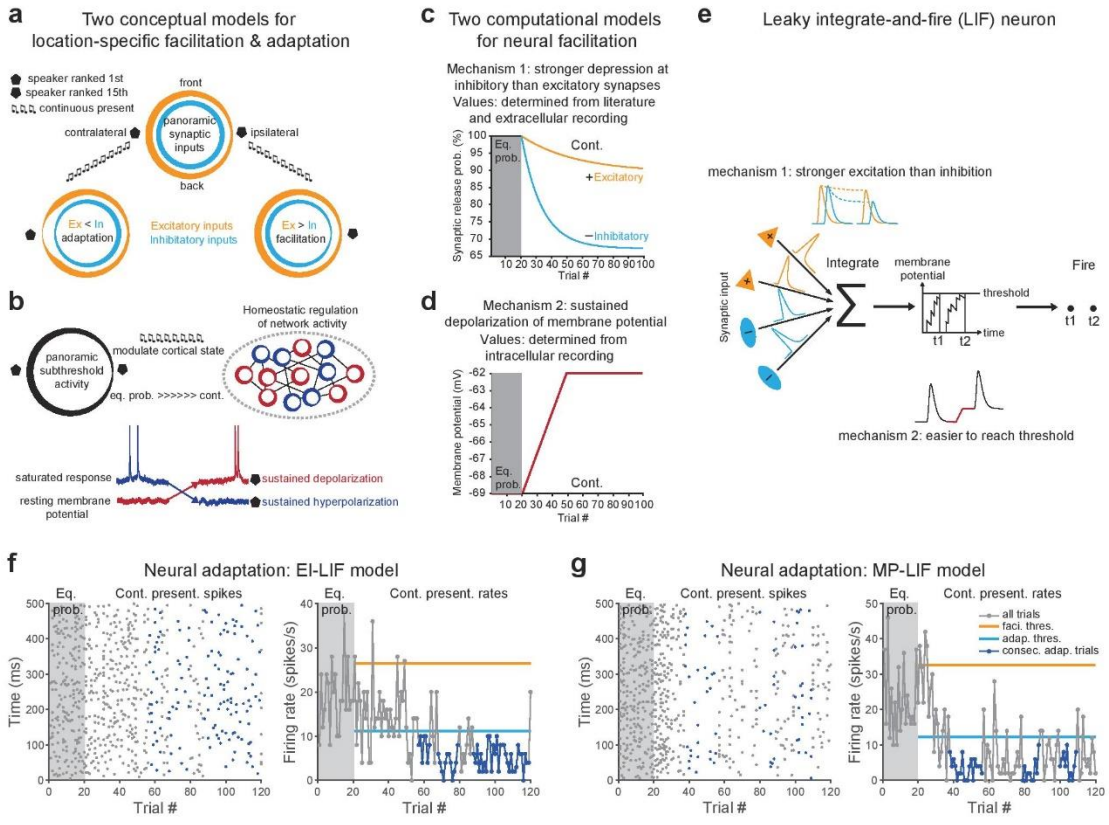

Extended Data Fig. 8 Explanations of EI-LIF and MP-LIF models.

a, A conceptual model for location-specific facilitation and adaptation. Orange and blue circles indicate excitatory and inhibitory synaptic inputs, respectively. The width of circles indicates the strength of synaptic inputs. Pentagon and upside-down pentagon shapes indicate 1st and 15th ranked speakers, respectively. Top, under equal-probability presentation mode, EI-LIF model neuron has a lower response at the ipsilateral location due to stronger inhibition (thick blue line) than excitation (thin orange line). Left, under continuous presentation mode, overall stronger inhibition than excitation would evoke neural adaptation at speaker ranked 1st (blue line is thicker than the orange line). Right, under continuous presentation mode, overall stronger excitation than inhibition would evoke neural facilitation at speaker ranked 15th (orange line is thicker than the blue line). **b,** A conceptual model for location-specific sustained depolarization and hyperpolarization. Left, under equal-probability presentation mode, MP-LIF model neuron has panoramic subthreshold activity across all spatial locations but activity at the ipsilateral location is weakest (width of circle). Right, the neural activity of the network is homeostatically regulated: some neurons exhibit sustained depolarization (red circles) while others exhibit sustained hyperpolarization (blue circles). Black lines indicate the connections between two neurons. Bottom, under continuous presentation mode, sustained depolarization of weaker responses (red line) at the 15th-ranked speaker will be accompanied by sustained hyperpolarization of stronger responses (blue line) at the 1st-ranked speaker. **c,** A computational model for location-specific facilitation. Gray shaded area (trial #1 to #20) indicates the equal-probability presentation mode. Under this presentation mode, no

adaptation occurred for both excitatory and inhibitory synaptic inputs, thus the synaptic release probability is 100% for both inputs. Under the continuous presentation mode (trial #21 to #100), the inhibitory synapses (blue line) have a stronger adaptation amplitude (i.e., lower synaptic release probability) than the excitatory synapses (orange line).

d, A computational model for location-specific sustained depolarization. Under the equal-probability presentation mode, the membrane potential is stable at -69mV. Under the continuous presentation mode, membrane potential reached a stable level of -62mV which was 7mV depolarized after 30 trials. Those three parameters were obtained from our intra-cellular recordings.

e, Leaky integrate-and-fire (LIF) neuron model. LIF neuron integrates multiple excitatory (orange lines) and inhibitory (blue lines) synaptic inputs and fires a spike (t1, t2) whenever the membrane potential passes the threshold. Top, location-specific facilitation mechanism for the EI-LIF model neuron. Bottom, the other mechanism for the MP-LIF model neuron.

f, Neural adaptation simulated by EI-LIF model neuron. Left, spike raster plot of one session under equal-probability (shaded area) and continuous presentation mode. Blue dots indicate spikes belong to the long adaptation phase (i.e., at least five consecutive trials with firing rates lower than the adaptation threshold). Right, trial-by-trial firing rate from the same session. Blue dots and line indicate trails belong to the long adaptation phase. Thick orange and blue lines indicate the facilitation and adaptation thresholds, respectively.

g, Similar to **f** but for MP-LIF model neuron.

Name	Symbol	Source	Value	Range
Leaky integrate-and-fire (LIF, equation 1)				
Time step	Δt	This model	0.0001s	fixed
Capacitance	C	Wehr and Zador 2003	0.25*10^{-9}F	fixed
Excitatory reversal potential	E_e	Wehr and Zador 2003	0V	fixed
Inhibitory reversal potential	E_i	Wehr and Zador 2003	-0.085V	fixed
Leak conductance	g_{rest}	Wehr and Zador 2003	25*10^{-9}S	fixed
Resting potential	E_{rest}	Experimental data	-0.069V	fixed (EI-LIF)
Spontaneous noise scale	σ_s	This model	0.01V	fixed
Gaussian noise	ω_n	This model	[-1: 1]	random
Threshold above resting potential	V_{th}	Wehr and Zador 2003	0.02V	fixed
Excitatory and inhibitory conductance (equations 2 and 3)				
Excitatory synaptic release probability	P_{rel_e}	This model	1	fixed (MP-LIF)
Inhibitory to excitatory ratio	r	This model	1	fixed
Excitatory synaptic input number	N_e	Wehr and Zador 2003	10	fixed
Alpha function time constant	τ	Wehr and Zador 2003	0.005S	fixed
Conductance noise scale	σ_c	This model	2.5*10^{-8}S	fixed
Inhibitory synaptic release probability	P_{rel_i}	This model	1	fixed (MP-LIF)
Inhibitory synaptic input number	N_i	Wehr and Zador 2003	10	fixed
Inhibitory to excitatory delay	d	This model	0S	fixed
Excitatory and inhibitory synaptic depression model (EI-LIF) (equations 4 and 5)				
Excitatory synaptic depression amplitude	A_e	This model	0.003	fixed
Excitatory synaptic time constant	τ_e	This model	20S	fixed
Probability of target speaker	P_s	Experimental data	1/0.75/0.5 0.25/0.07	fixed
Inhibitory synaptic depression amplitude	A_i	This model	0.025	fixed
Inhibitory synaptic time constant	τ_i	This model	10S	fixed
Stimulus count	N_{SC}	Experimental data	36	fixed
Trial step	T	This model	1	fixed
Number of trials in random mode	T_r	This model	20	fixed
Number of trials in continuous mode	T_c	This model	300	fixed
Membrane potential depolarization and hyperpolarization model (MP-LIF) (equations 6 and 7)				
Dynamic resting membrane potential	E_{rest_MP}	Experimental data	-0.062V -0.076V	max min
Membrane potential polarization value	M	Experimental data	±0.007V	max, min
Number of trials to stabilize	T_{th}	Experimental data	30	fixed
Spike threshold scale	S	This model	0.3	fixed
Stimulus count	N_{SC}	Experimental data	30	fixed

Extended Data Table. 1 Parameters and corresponding values used in EI-LIF and MP-LIF model neurons.